TITLE: Rotational and Vibrational Temperature Measurements in the LDR High Enthalpy Shock Tunnel HEG Using LIF and Flash Lamp Absorption

Rotational and Vibrational Temperature Measurements in the DLR High Enthalpy Shock Tunnel HEG Using LIF and Flash Lamp Absorption

W. H. Beck
Aerothermodynamics Section,
Institute of Fluid Mechanics,
German Aerospace Center (DLR),
Bunsenstraße 10,
37073 Göttingen
Germany

ABSTRACT

Use of LIF in two line thermometry TLT and of flash lamp absorption to examine high enthalpy flows is presented. The aim is to measure rotational and vibrational temperatures of nitric oxide NO in high temperature air in the Göttingen High Enthalpy Shock Tunnel HEG. Theory of NO (energy levels, spectroscopy, level populations), LIF and TLT are discussed. Results are given from a test cell to validate TLT with NO LIF as a quantitative technique. HEG results for rotational and vibrational temperatures in the free stream and around models are presented. Finally, flash lamp absorption results yielding these temperatures are given.

1. INTRODUCTION

High enthalpy flows such as in the High Enthalpy Shock Tunnel HEG of the DLR in Göttingen are characterised by very high temperatures where the test gas (usually air) is dissociated and where the concentrations of the atomic and molecular species may not correspond to those pertaining to the translational temperature of the gas - this is chemical non-equilibrium. Furthermore, the gas may also not be in thermal equilibrium, i.e. internal temperatures (electronic, vibrational and in some cases even rotational temperatures) may be different from each other and from the translational temperature. In the worst case, the levels may not be occupied according to a Boltzmann distribution, so that an internal temperature is not even defined. To examine and understand the properties of such gases, it is no longer adequate to measure just bulk properties such as pressure or temperature; one must examine the gas at its molecular level, and preferably using a technique which is non-intrusive and does not influence or alter the gas propereties. Laser induced fluorescence LIF is such a technique. It has the further advantage of enabling 2D spatially resolved measurements of temperatures, as opposed to other techniques which measure line of sight (absorption techniques) or at a point (CARS).

A common component of high temperature air is nitric oxide NO. In HEG it is present up to levels of 10%. NO is a species which is quite well studied and understood (its energy levels, spectroscopy), and is well suited to LIF and absorption studies. This lecture will deal with basic theory of the NO molecule - its structure, energy levels, level populations, spectroscopy and its use in two line thermometry TLT using LIF. Although this theory is universal, pertaining not only to LIF work, it will be presented with mainly this aim in mind. Experimental apparatuses for LIF (laser apparatus, test cell) and the facility HEG will be described. Emission spectra in HEG are shown to prepare the way for use of planar LIF (PLIF) around models in the gas flow. A discussion of detailed experiments in a heated test cell containing NO, necessary to establish the requirements for quantitative TLT, follows. HEG LIF results are presented in two groups: LIF measurements of rotational and vibrational temperatures in the HEG free stream, and in flows around models (HERMES, cylinder, sphere, blunted cone, HOPE). Finally, results using flash lamp absorption in the HEG will be presented.

Paper presented at the RTO AVT Course on "Measurement Techniques for High Enthalpy and Plasma Flows", held in Rhode-Saint-Genèse, Belgium, 25-29 October 1999, and published in RTO EN-8.

2. THEORY

This chapter will overview some important theoretical concepts concerning the energy levels and spectroscopy of the NO molecule, the laser induced fluorescence technique and its use to determine internal (rotational and vibrational) temperatures via two line thermometry TLT. It will and cannot be an exhaustive overview, but rather will summarise the basics (there are several texts and literature references given in Ref. 1 which go into far greater detail). Above all, an attempt will be made to stress those points which are important in applying TLT to high enthalpy flows.

2.1 The NO molecule

The linear combination of atomic orbitals approach to forming the molecular orbitals (MO) of NO leads to an electron configuration in the electronic ground state (GS) where the last (outermost) electron resides in an anti-bonding $\pi^*_{(g)}$ molecular orbital. This is a single unpaired electron, so that the multiplicity of the GS is 2. The promotion of this electron can occur to higher (in energy) MO's, for example through absorption of a photon of light. The excited NO molecule can relax back to its GS via several processes, including emission of a photon of either the same or lower energy (fluorescence); all these processes are important in using LIF for TLT, and will be discussed later.

When an electron is boosted to a higher electronic level, it is also possible for the molecule to experience a change in its rotational and vibrational energies. (All internal energy changes are subject to certain selection rules, which arise out of parity and symmetry considerations pertaining to dipole transitions.) The energy of the molecule, or rather the energy change following a particular transition, can be broken down into electronic n, vibrational v and rotational J components - the so-called term energies T(n,v,J). Each state of the molecule, and its term energy, are uniquely defined by so-called quantum numbers, numbers which arise out of the wave function solutions (eigen functions) of the Schrödinger equation.

It is customary to represent pictorially these term energies, including the vibrational (and rotational) manifolds, in a potential energy level diagram such as in Fig. 1 for NO (see Ref. 1).

Here the energy (in units wavenumbers cm^{-1}, 1 ev ≡ 8067 cm^{-1}) of the level is plotted against internuclear separation (in Angstroms Å, 1 nm ≡ 10 Å) between N and O atoms in the molecule. The various electronic states are given term symbols, starting with X for the GS, and then A, B, C, ... for the higher lying states. Each electronic energy level is represented by either direct or projected quantum numbers, and given either a Greek symbol or value; e.g. the GS $^2\Pi^+_{mJ}$ has total spin ½, therefore multiplicity 2, total orbital angular momentum L = 1, hence Π state, and a projection of the summed orbital and spin quantum numbers m_J, with values of 1/2 or 3/2.

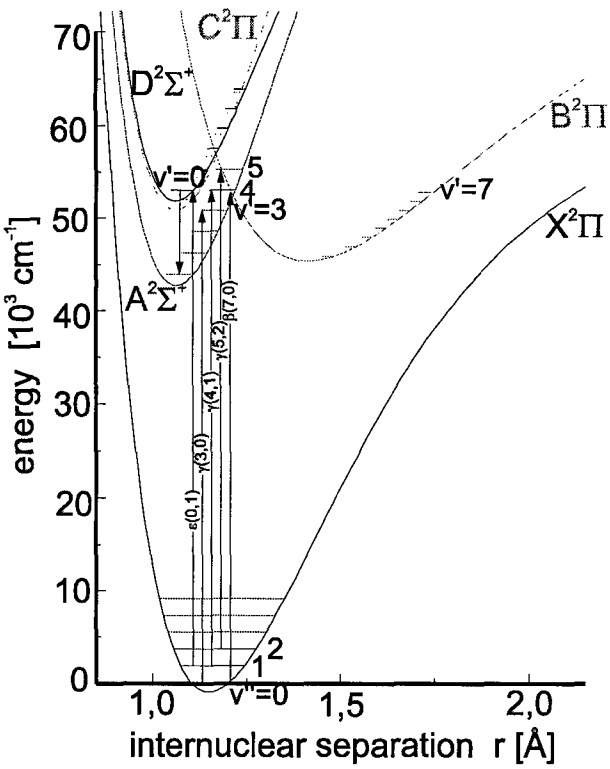

Fig.1 Potential energy level diagram for NO.

The above picture considers only the electronic, and not the rotational energy levels; there exists a coupling between the nuclear rotation and the electron movement, leading to a further splitting of the energy levels, the so-called Λ-splitting. Hence, when considering transitions from a particular

rotational level in the GS, they can arise from four energy levels, each having a (sometimes only slightly) different energy. Selection rules for rotational transitions allow only quantum number changes ΔJ of -1, 0, +1 ($J \neq 0$), and only transitions to states of opposite parity, so that in all 12 separate transitions (spectral lines) to a Σ-excited state (where $m_J = 0$) can arise from one GS rotational level. This can be seen in Fig. 2. Of the four major NO electronic energy levels, X, A, B. C and D, as shown in Fig.1, only the X, A and D will be of main interest here. Whereas the vibrational energy levels (v = 0, 1, 2,....) are shown, the rotational manifolds (see Fig. 2) superimposed on each vibrational level, with their even smaller energy spacings, are not shown.

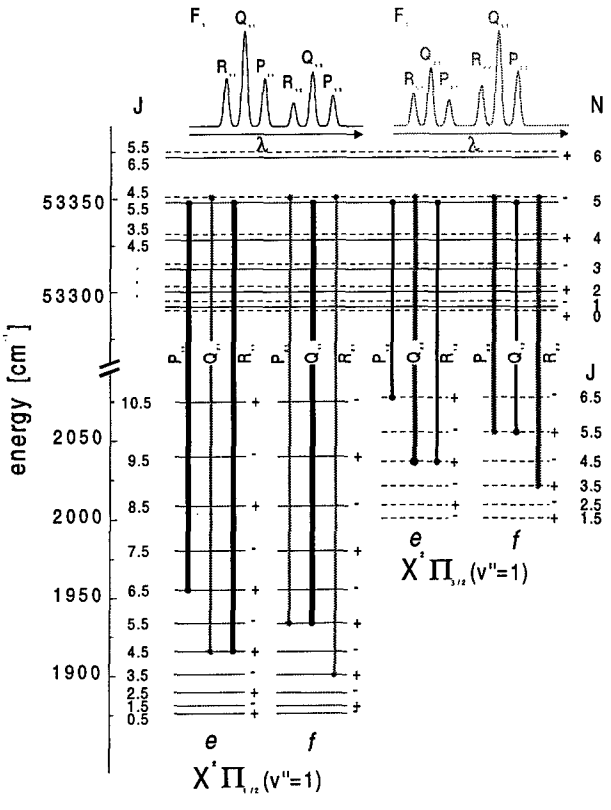

Fig. 2 $\Sigma \leftarrow \Pi$ transitions in NO, showing 12 branches.

Transitions between the states D ← X and A ← X are given designations ε and γ, respectively, with the upper and lower vibrational quantum numbers v being given in brackets; e.g. $\varepsilon(0,1)$ refers to the transition between the X ground state, v = 1, to the excited state D, v = 0. No information regarding the change in rotational quantum number J is included yet. This is represented as $\Delta J_{F,F'}(J")$, where ΔJ = -1, 0 or +1 (see before) is represented by the letter P, Q or R, F' and F" represent the two m_J values 1/2 and 3/2, respectively, and J" represents the rotational level in the GS from which the transition arises. (The energy levels and transitions of NO are summarised in some more detail in ref. 1, where literature references can be found.) The two laser-excited transitions used for the LIF to be discussed later are $\varepsilon(0,1)$ $R_{22}(27.5)$ and $\varepsilon(0,1)$ $(R_{21}(17.5) + P_{11}(35.5))$; whereas the first transition is a single line, the second is an overlap of two lines which can lead to errors at temperatures above 1000 K, if not properly accounted for - see later. In the case of flash lamp absorption, where both low resolution vibrational bands (rotational envelopes) and high resolution rotationally-resolved lines are measured from broadband absorption experiments, vibrational transitions (0,0), (1,0) and (0,1) and low-lying rotational levels ($J \approx 4.5$) are involved.

2.2 Thermal populations

Given that thermal equilibrium between the electronic, vibrational and rotational levels exists, the fraction f of the total population in a given energy level |n,v,J> is given by:

$$f(n,v,J,T_{int}) = g_n \frac{g_{rot}}{Q(T_{int})} \; e^{-\left[\frac{T(n,v,J,T_{int})}{kT}\right]}$$

where g_n is the electronic degeneracy, g_{rot} the rotational degeneracy (= 2J + 1), k Boltzmann's constant, $Q(T_{int})$ the total partition function and T_{int} the internal temperature, so called to distinguish it from the translational temperature T_{trans}, which may or may not be the same - see later. Hence, for a given known molecule with known properties and energy levels, the thermal distribution can be represented by just one variable, the temperature T_{int}. For the case of the rigid rotor, the term energy can be split into a sum of electronic, vibrational and rotational components and the partition function into a product of components from these modes. The fraction f can be redefined as:

$$f(n,v,J,T_{el},T_{vib},T_{rot}) =$$

$$g_n(2J+1)\frac{e^{-\left[\frac{T_{el}(n)}{kT_{el}}\right]}}{Q(T_{el})}\frac{e^{-\left[\frac{T_{vib}(v)}{kT_{vib}}\right]}}{Q(T_{vib})}\frac{e^{-\left[\frac{T_{rot}(J)}{kT_{rot}}\right]}}{Q(T_{rot})}$$

Hence, as can be seen from the above equation, it is possible that T_{el}, T_{vib} and T_{rot} are different, and also different from T_{trans}. However, the existence of a temperature as a variable requires a Boltzmann distribution - no Boltzmann distribution, no temperature defined! All spectroscopic methods used to determine internal temperatures rely on this assumption. Given that it holds, one can also see how to measure internal temperatures - measure the population in two different (e.g. rotational) levels, from which the (e.g. rotational) temperature can be determined.

To see how these populations change as a function of temperature can best be seen using two examples for NO, one for vibrational and one for rotational population distributions. Fig. 3 is a plot of fraction of vibrational level population (normalised to v = 0 at 300 K) plotted against temperatures up to 6000 K.

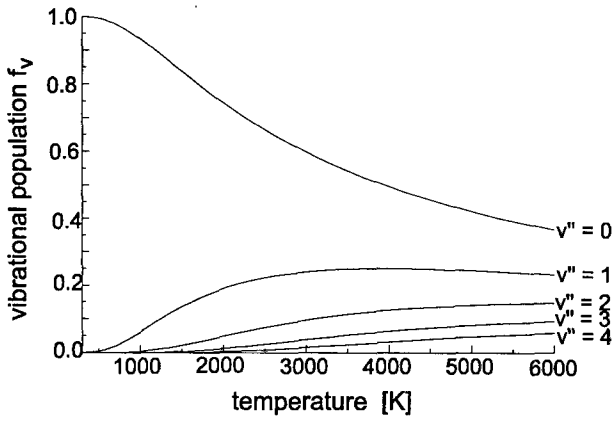

Fig. 3 Vibrational population fraction f_v for various NO vibrational levels as a function of temperature.

At HEG free stream temperatures of less than about 1100 K, one can see that only levels v = 0 and 1 are substantially populated. In fact, the aforementioned ε-bands arise from v = 1, so that these transitions cannot be used at temperatures below about 600 K. Behind shocks in HEG temperatures can be as high as 9000 K, but at these high temperatures one sees another problem, which is best exemplified by the following: if one measures populations in levels, say, v = 2 and 3 at temperatures around 5000 K, one can see that the ratio of the populations in these levels is quite temperature insensitive. Or put another way, the demands on accuracy in measuring these populations are very high.

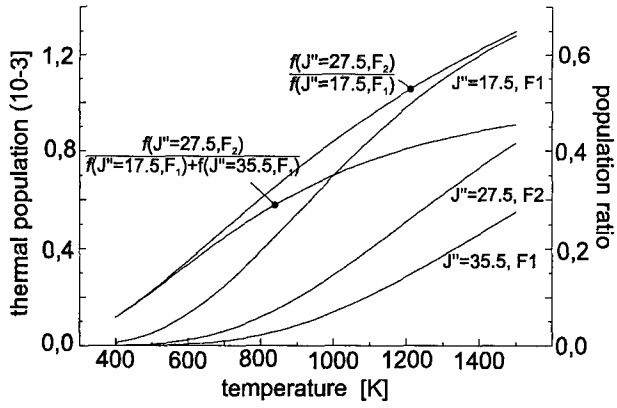

Fig. 4 Rotational population fractions and ratios for two NO rotational levels as a function of temperature.

The second example, shown in Fig. 4, is a plot of population fraction of the two NO rotational levels J" = 17.5 and 27.5 discussed in chapter 2.1 (and of the level J" = 35.5) against temperatures up to 1500 K. Also plotted are the ratios of the two populations with and without consideration of the J" = 35.5 level ($f_{27.5}/(f_{17.5}+f_{35.5})$ and $f_{27.5}/f_{17.5}$, respectively).

Neglecting the contribution from J" = 35.5, one can estimate from the ratio $f_{27.5}/f_{17.5}$ the accuracy of rotational temperature T_{rot} determination: taking the ratio for the case T_{rot} = 1000 K, and assuming an error in ratio measurement of 10% (quite good for single shot measurements - see later), one obtains an error in T_{rot} of about 7%. Hence, these two transitions, based on only this criterion, are quite good for measurements at around 1000 K, although it is clear from Fig. 4 that the J" = 35.5 contribution cannot be neglected at higher temperatures. These matters will be further discussed in chapter 2.4.

2.3 LIF - two and three level approaches

The method whereby one obtains the abovementioned level populations needs to be looked at more closely. This is best done using the two level LIF model: in brief, a laser is used to excite NO from a lower level to an excited state, from whence a measurement of the intensity of re-emitted fluorescence can be related to the original population in the ground state. The requirements for this to apply, and the complications that may arise, will be discussed here briefly. Fig. 5 shows a two level system involving two states |1> and |2>, representing (v,J) levels in the NO X and D electronic states, respectively

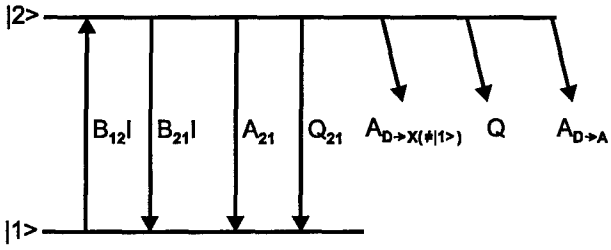

Fig. 5 Two-level LIF model for NO.

In the case of weak laser excitation, where the fluorescence signal F_{lin} is proportional to laser intensity, one can write (see ref. 1, and references therein):

$$F_{lin} = B_{21} E^{las} g N f \frac{A_{21}}{A_{21} + Q_{21}},$$

where where B_{21} and A_{21} are Einstein coefficients for stimulated and spontaneous emission from state |2> to |1>, respectively, Q_{21} is the radiation-less channel for level |2> de-population, E^{las} is the laser energy, g is the spectral overlap integral for absorption (representing the coincidence and bandwidths of spectral transition and laser - $g = g(\nu_{abs}, \Delta\nu_{abs}, \nu_{las}, \Delta\nu_{las})$), N the NO density and f the Boltzmann fraction for the lower level. The term

$$q_F = \frac{A_{21}}{A_{21} + Q_{21}}$$

is called the quantum yield, and lies between 0 and 1, depending on how strongly the fluoresence radiation is reduced (quenched) by other processes. In the two level model, Q_{21} in the above equation actually represents all processes not leading to re-emission back to level |1>, viz. Q_{21}, $A_{D\text{-}X(\neq|1>)}$, Q and $A_{D\text{-}A}$ in Fig. 5.

In the LIF experiments fluorescence signals S_f are recorded using either image-intensified cameras or photomultipliers. S_f is related to F_{lin} by

$$S_f = F_{lin} V \eta \frac{\Omega}{4\pi},$$

where V is the measurement volume, η is the detection sensitivity (gain, filter losses, etc.) and $\Omega/4\pi$ is the detection solid angle.

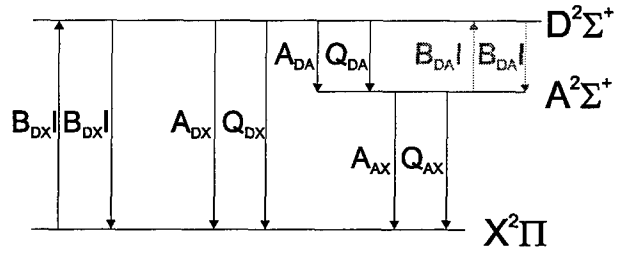

Fig. 6 Three-level LIF model for NO.

The proximity of the NO A state to the D state, shown in Fig. 1, complicates the situation, since it is also involved in energy transfer and removal processes - $A_{D\text{-}X(\neq|1>)}$, and $A_{D\text{-}A}$ - which influence the proportionality of fluorescence signal to level population. A three level system including the NO A state is shown in Fig. 6.

Here all processes for populating (absorption $B_{DA}I$) and depopulating (spontaneous emission A_{DA}, stimulated emission $B_{DA}I$ and collisional quenching Q_{DA}) the upper D state, and also corresponding processes between the A and X states (spontaneous emission A_{AX} and quenching Q_{AX}) need to be considered. Furthermore, at higher laser power densities and higher NO densities, a particularly efficient process called amplified spontaneous emission ASE provides an efficient channel for energy removal from the D state. (This process arises from the strong pumping of the D state, leading to a population inversion between D and A states, which produces an amplification of D → A transitions in the direction of the D ← X

pump laser beam.) Clearly all this can become quite complex if all processes occur, but on the other hand, if one is not aware of them, using LIF to do quantitative TLT can lead easily to erroneous results.

2.4 Two line thermometry TLT

To determine temperatures, fluorescence signals S_f arising from excitation from two different lower energy levels |1> and |2> are measured, e.g. using the transitions ε(0,1) $R_{22}(27.5)$ and ε(0,1) ($R_{21}(17.5)$ + $P_{11}(35.5)$) one would obtain a rotational temperature. A ratio of energy and wavelength corrected signals is formed:

$$R = \frac{S_{f,1} / E_1^{las} g_1}{S_{f,2} / E_2^{las} g_2} = \frac{B_{21,1} N f_1(E_1,T) V_1 \eta_1 \frac{\Omega_1}{4\pi} q_{F,1}}{B_{21,2} N f_2(E_2,T) V_2 \eta_2 \frac{\Omega_2}{4\pi} q_{F,2}}$$

Cancelling, grouping together temperature-independent constants (molecular and apparatus constants) and assuming there is no quantum level dependence of quenching ($q_{F,1} = q_{F,2}$) leads to

$$R = c\, e^{-\frac{\Delta E}{kT}},$$

where $\Delta E = E_2 - E_1$ is the energy separation of the two states from which excitation occurred. To obtain the temperature T, a calibration measurement in a test cell at known NO concentration and temperature T_{cal} and using the same experimental setup as for HEG is carried out: $R_{cal} = c e^{-(\Delta E/kTcal)}$. Setting the value T_0 for the characteristic temperature of the two states ($T_0 = \Delta E/k$), one obtains the measured temperature T:

$$T = \left\{ \frac{1}{T_{cal}} - \frac{1}{T_0} (\ln R - \ln R_{cal}) \right\}^{-1}.$$

For the case that $T_{vib} \neq T_{rot}$, the expression for R becomes

$$R = c\, e^{-\frac{\Delta E_{vib}}{kT_{vib}}} e^{-\frac{\Delta E_{rot}}{kT_{rot}}}.$$

If one temperature is known, the other can be determined in a measurement as described above.

One needs to ask the question: under which conditions and with which assumptions do the above equations apply when carrying out single shot TLT in high enthalpy flows? They are:

1. *Linear fluorescence* - requires laser excitation to be weak.
2. *No unaccounted-for loss processes* - mass balance between the two levels must apply: N_1+N_2=constant.
3. *No RET* - rotational energy transfer (RET) in the ground state, falsifying the required thermal population, must be low (this needs be considered behind strong shocks in HEG).
4. *Rotational dependence of quantum yields* - should not exist, or must be known and quantified.
5. *Laser pulse time form* - should be as near to rectangular as possible (does not apply fully to the ArF excimer lasers used in HEG).
6. *Fluorescence reabsorption* - in the path through the HEG test gas from excitation volume to the detection system must be negligible (hence any fluorescence ending in the v = 0 level of the X ground state must be suspect).
7. *Laser beam absorption* - from the HEG test section window to the excitation volume must not occur (exciting the ε-bands originating from v = 1 reduces this problem, but even v = 1 becomes populated at T > 600 K - see Fig. 3).
8. *Calibration cell conditions* - must be such that the calibration results can be carried over and used for comparison with the HEG results.
9. *Boltzmann distributions* - must exist! This assumption is the crux of both LIF and flash lamp absorption measurements.

The sensitivity of TLT is given quite simply by

$$\frac{\Delta T}{T} = \frac{T}{T_0} \frac{\Delta R}{R} = \frac{T}{1310} \frac{\Delta R}{R},$$

where the value T_0 = 1310 K has been inserted for the two rotational levels J" = 17.5 and 27.5 for the transitions ε(0,1) $R_{22}(27.5)$ and ε(0,1) $R_{21}(17.5)$. One sees immediately that at temperatures above about 1000 K the relative accuracy of the ratio R measurement approaches that of the temperature sensitivity, so that, for a 5% temperature accuracy, one needs an accuracy of 5% in R or about 3-4% in S_f. This is not difficult in cases where signal averaging can be used, but for single shot work as

in HEG where the short test time of 1 ms allows only one laser shot from each of the two lasers, this is most demanding. A general requirement for greater temperature sensitivity arises out of the above: $T << T_0$. This is desirable, but, as in the case of HEG (see later), not always possible to achieve.

3. EXPERIMENTAL TOOLS

3.1 The High Enthalpy Shock Tunnel HEG

The HEG is a free-piston driven shock tunnel operating in the reflected shock mode. It has been described in greater detail elsewhere (ref. 2). As shown in Fig. 7, a reflected shock creates high temperature and pressure conditions in the reservoir (before the nozzle entrance), after which the test gas expands through the nozzle to deliver the free stream conditions in the test section. The test time is about 1 ms. Also shown in Fig. 7 are nominal conditions which have been calculated using a non-equilibrium Euler code for the free stream and the reservoir - these conditions apply to the old contoured nozzle in HEG, with which most of the LIF testing was carried out. Conditions I and III are low pressure, with high and low specific enthalpy, respectively, and II and IV are high pressure, also with respective high and low enthalpies. Free stream temperatures are calculated to lie between about 500 and 1100 K and NO concentrations are quite high, lying between about 1 and 8 x 10^{15} cm^{-3}.

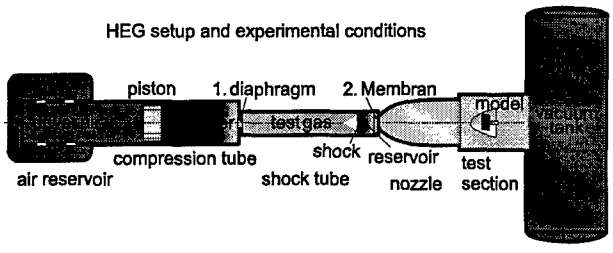

Nominal conditions for the contoured nozzle

Conditons		I	II	III	IV
p_0	[MPa]	40	90	45	110
T_0	[K]	9100	9700	7300	8100
T_∞	[K]	790	1040	550	720
h_0	[MJ/kg]	21	22	13	15
u_∞	[km/s]	5,9	6,2	4,8	5,1
N2	[10^{15}cm^{-3}]	26,1	56,6	44,0	95,6
O2	[10^{15}cm^{-3}]	1,1	4,3	7,6	18,0
NO	[10^{15}cm^{-3}]	1,1	3,0	3,9	8,4

Fig. 7 The High Enthalpy Shock Tunnel HEG.

3.2 The heated calibration and test cell

A special NO-containing test cell was designed and constructed to carry out NO spectroscopy measurements, to check the various assumptions and approximations in using TLT, to carry out time resolved measurements on NO quenching and to check imaging techniques when using 2D spatially resolved PLIF (Planar LIF). Several design criteria had to be met: 1. Temperatures encompassing the HEG free stream range - the cell can be heated up to 1300 K, 2. NO concentrations as in HEG free stream, and even lower to check quench-free conditions; 3. Optical access through large windows to permit laser beam traversal and imaging of 2D LIF signals using image intensified CCD cameras (ICCD's); 4. A flow system to ensure NO in the test volume is replenished regularly; 5. Appropriate gas path and sizing to make sure the gas temperature is as high as the heated ceramic tubing (where the thermoelement temperature is measured) and is homogeneous; 6. Design of cell geometry to enable it to be placed in the HEG test section for LIF calibration purposes. (5. is difficult at very low NO pressures.) The test and calibration cell is shown in Fig. 8 in position in the HEG test section.

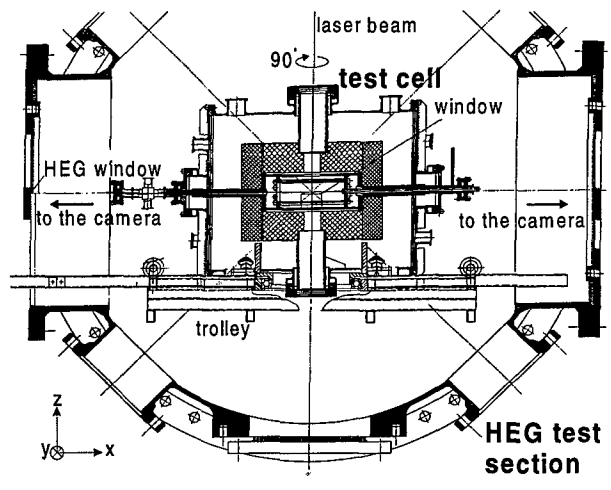

Fig. 8 Calibration and test cell shown installed in the HEG test section.

The view is shown in flow direction in HEG. The cell is introduced via a trolley into the test section and rotated 90° so that both windows face the test section openings left and right. Laser beams enter top and bottom. More details on the test cell are to be found in Ref. 3.

3.3 The LIF laser apparatus for HEG

The LIF apparatus, as used on HEG, is shown in Fig. 9. (It is described in more detail in Ref. 1.)

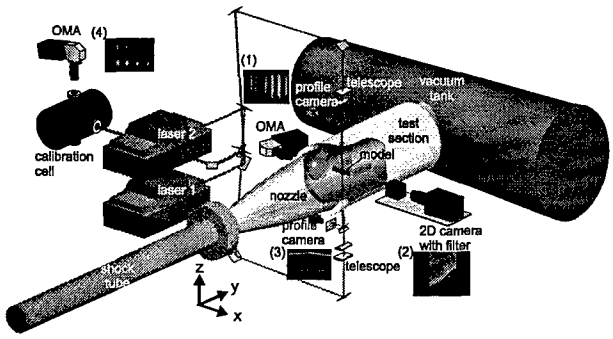

Fig.9 The HEG LIF apparatus.

Two formed (e.g. as sheets) laser beams from tunable ArF excimer lasers, operating at a wavelength tunable in the range around 192.9 - 193.9 nm, counter propagate through the test section in the vertical direction. Some percentage of each beam is split from the main beam and diverted into the calibration cell for spectroscopy checks and calibration purposes. A small proportion of each beam is also split off and recorded on an energy monitor (CCD camera). The lasers are thereby tuned to appropriate NO transitions and are fired one after the other with a small time delay (~µs), and the ensuing fluorescence is imaged with a UV lens either directly onto an ICCD for 2D fluorescence images or onto the slit of a spectrometer coupled to an ICCD (functioning as an optical multichannel analyser OMA) for spectrally resolved images (see images (2) and (1), respectively, in Fig. 9).

3.4 The LIF laser apparatus for the test cell

Much testing of TLT for HEG was carried on an HEG mock-up, consisting of the calibration cell discussed in chapter 3.2 representing HEG and a further simpler test cell as calibration and reference cell. Energy momitors, as described in chapter 3.3, are also installed here. The setup with just one laser is shown in Fig. 10.

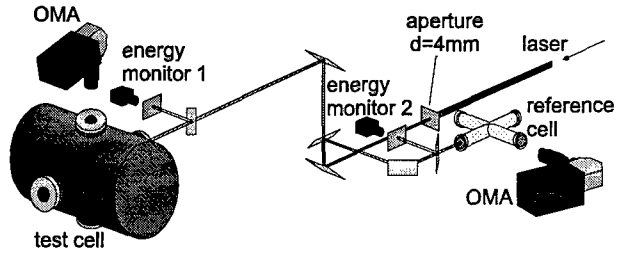

Fig,10 The LIF apparatus for tests in the calibration cell.

3.5 Filter for LIF measurements behind shocks

The captured NO fluorescence signals after laser excitation at ~193 nm extend over a UV wavelength range of about 193 - 300 nm. To reduce influences in HEG from emission behind shocks (see chapter 4), it was necessary to have special optical filters made which are tunable over a small range in the deep UV, have high suppression factors (~10^6) and avoid fluorescence signal distortion so that imaging can be carried out. The compound filters consist of four reflection interference filters in a configuration as shown in Fig. 11; by varying the angle α over the range 30 to 50°, the reflection band width profile shifts as shown the figure, lower left. The corresponding change of the measured fluorescence spectrum from the NO laser-excited

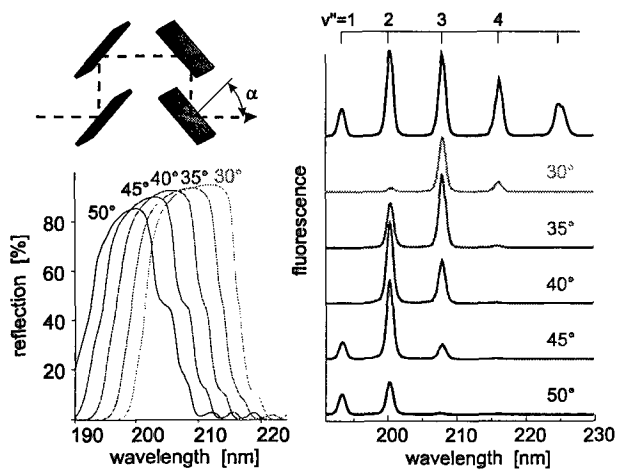

Fig.11 Filter to reduce background radiation in HEG LIF measurements.

transition $\varepsilon(0,1)$ $R_{22}(27.5)$ for these filter angles can be seen to the right of the figure.

4. EMISSION SPECTRA IN HEG

The gas temperature in the shock-heated region in front of a cylinder at enthalpies of 22 MJ kg^{-1} can be as high as 9000 K. The gas radiates very strongly. To examine this emission, and to ascertain what needs to be done to carry out LIF in this difficult region, emission spectra in front of a cylinder in an N_2 flow were measured over a set of HEG runs at high enthalpy. The spectra were normalised and packed together to give a composite emission spectrum over the total wavelength range of 180 - 850 nm. This measured spectrum is shown as 1 in Fig. 12.

Superimposed (2) is the NO fluorescence spectrum shown in Fig. 11 (not to scale), with an arrow (↓) indicating the excitation wavelength. One can see that at wavelengths above about 220 nm the emission is so strong that it would make extracting NO fluorescence signals nigh to impossible. The role of the filters discussed in chapter 3.5 and shown in Fig. 11 is to suppress substantially this emission above about 220 nm.

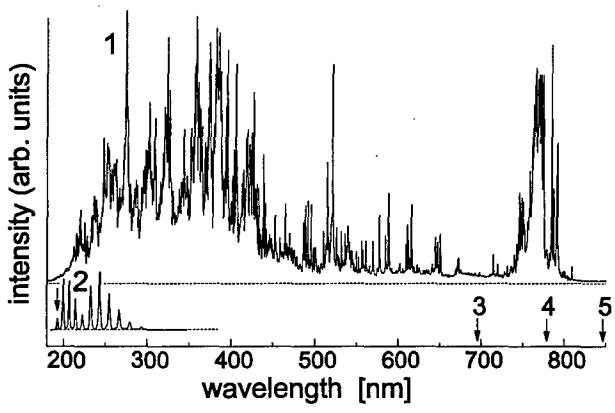

Fig.12 Emission spectrum (1) of radiating gas behind the shock in front of a cylinder in a high enthalpy N_2 flow in HEG. An unscaled NO fluorescence spectrum is shown for comparison.

If one can identify the source of the profuse emission seen in Fig. 12 between about 220 and 600 nm, one may be able to reduce it. Fig. 13 (upper trace, 1) shows an excerpt from the spectrum in Fig. 12 over the wavelength range of 350 - 390 nm. Shown below are calculated spectra for iron FeI and FeII species at temperatures of 6000 (2a), 9000 (2b) and 12000 K (2c).

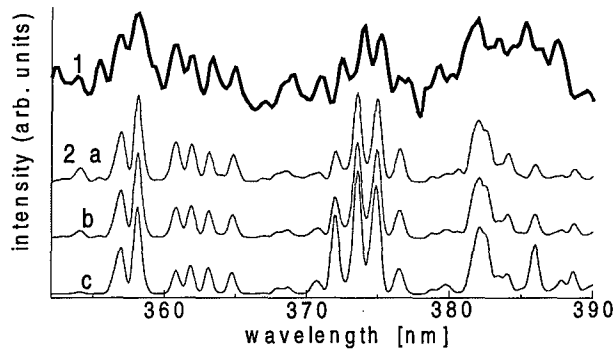

Fig.13 Measured emission spectrum (1) compared with calculated Fe spectra at different temperatures: 2a. 6000 K; 2b. 9000 K; 2c. 12000 K.

The coincidence of line wavelengths is quite good (e.g. 355 - 365 nm; 370 - 377 nm), but there are clearly unidentified lines still present (e.g. 379 nm; 388 nm). The relative insensitivity of the calculated spectra to vast changes in temperature suggests that the technique of emission spectroscopy is not suited to temperature determination in these shock heated gases. The abundance of Fe lines is not surprising; in *any* hypersonic facility at high enthalpies there is ablation of material (in HEG in the shock tube), which is carried by the gas flowing through the nozzle and into the test section. The presence of this material in the flow is an unavoidable evil in shock tunnels, making optical work difficult (depending on wavelength) and affecting heat transfer measurements at high reservoir pressures. The effect can be reduced somewhat by using other materials than steel (the source of Fe), such as copper alloys, but generally it can't be fully removed and has to be contended with.

5. LIF RESULTS FROM THE TEST CELL

The spectroscopy of NO after laser excitation at 193 nm and most of the assumptions and approximations discussed in chapter 2.4 on TLT

have been exhaustively studied using an experimental setup as shown in Fig. 10. All this work will be exemplified by a few cases to be discussed here; much more detail is to be found in Ref. 1.

5.1 NO spectroscopy

A glance at the NO molecular energy levels in Figs. 1 and 2 shows that excitation at 193 nm is quite complex. Indeed, over the tuning range of the ArF excimer laser (~193.9 - 192.9 nm ≡ 51575 - 51850 cm^{-1}), some 400 transitions have been observed and identified in LIF measurements in the test cell (Ref. 1). Excitation spectra measured at temperatures 300, 500, 700 and 1000 K are shown in Fig. 14. At temperatures below 500 K only the v=0 vibrational state is appreciably populated, so that the β(7,0) (and γ(3,0)) transitions predominate. Above 500 K the ε(0,1) and γ(4,1) (and at even higher temperatures even γ(5,2)) transitions become stronger.

The transition line strengths for the ε-bands are about 10x stronger than either the β- or γ-bands, making them a logical choice for single shot work in HEG. (Their disadvantage lies in their quicker saturation at moderate laser power densities.)

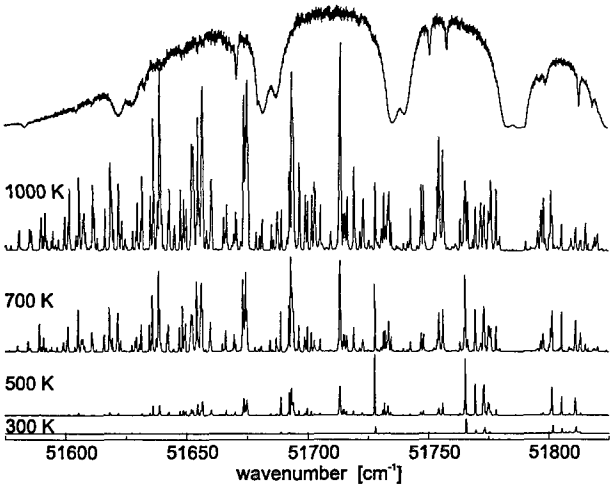

Fig.14 NO excitation spectra at various temperatures (upper trace - laser output showing O_2 absorption "holes").

Having identified the lines, one needs to establish the major criteria for suitable candidates for TLT in HEG:

1. *Laser energy* -the lines must lie in a wavelength region where there is sufficient laser energy, away from O_2 absorption bands;
2. *Electronic states* - due to their different fluorescence yields, these should be the same for both transitions;
3. *Line intensities* - should be high enough to be detected in single shot work, i.e. high Einstein coefficients and sufficiently populated levels;
4. *Single lines* - the lines should consist preferably of just one transition;
5. *Energy separation* - ΔE between the two lower quantum levels of the transitions must be as large as possible (see chapter 2.4);
6. *Vibrational temperatures* - can only be obtained from lines having different lower vibrational levels (obvious, but not trivial, since the tuning range of the lasers is very limited).

With these criteria, and taking into account the 400 identified transitions, not too many candidates appear: Two line pairs were chosen for TLT measurements in HEG, one for rotational temperatures T_{rot}:-

1. ε(0,1) $R_{22}(27.5)$	51696.2 cm^{-1}
2. ε(0,1) ($R_{21}(17.5) + P_{11}(35.5)$)	51636.5 cm^{-1}

and the other for vibrational temperatures T_{vib}:-

3. γ(3,0) $R_{11} + Q_{21}$ (45.5)	51746.7 cm^{-1}
4. γ(4,1) $R_{11} + Q_{21}$ (27.5)	51746.7 cm^{-1}

Wavenumbers of each transition are shown. The two transitions for T_{vib} determination are exactly coincident, so that both transitions are excited by the one laser pulse.

5.2 Fluorescence signal correction

In TLT using two lasers there will be differences in the energy, spatial and spectral (!) distribution of the two laser beams. These must be known or measured, and used to correct the fluorescence signals. 145 separate LIF measurements were carried using the setup of Fig. 10 with the test cell containing 100 Pa NO and at a thermoelement temperature T_{therm} of 980 K for each of the two

transitions 1. and 2. identified before in chapter 5.1. Fluorescence signals were either left uncorrected, corrected with an energy monitor or corrected with the fluorescence signal obtained from the second reference cell (with 500 Pa NO and T_{therm} = 610 K). Each of the fluorescence signals from the one transition was combined with each of the other transition, so that 145^2 (=21025) fluorescence ratios and therefrom temperatures could be determined. These are plotted as temperature histograms in Fig. 15.

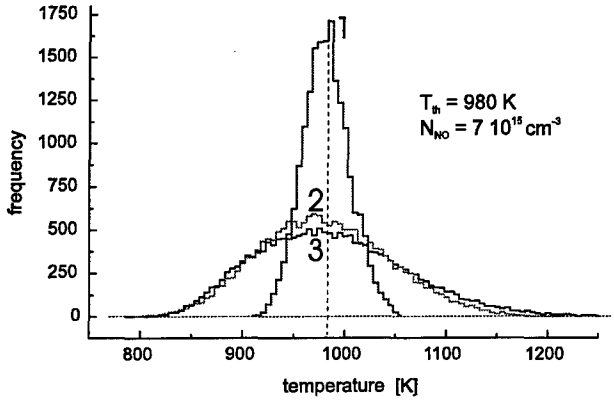

Fig.15 Temperature histograms for corrected and uncorrected LIF signals.

Histograms 1, 2 and 3 pertain to correction using reference cell fluorescence, energy correction and no correction, respectively. An energy correction alone obviously is hardly an improvement, so that, especially in single shot work, a reference fluorescence correction is mandatory.

5.3 Fluorescence reabsorption

The fluorescence from the laser excited NO in the test volume must usually pass through regions containing NO which can reabsorb the fluorescence, hence falsifying the signals. Its effect must be known. To examine this, transmission of fluorescence through the test cell at various NO densities and at a temperature of 1050 K was measured for emission to the lower vibrational levels v" = 1, 2, 3 and 4. The laser-excited transition 1. (chapter 5.1) was used. Results are shown in Fig. 16, where fluorescence normalised to the value for v" = 4 is plotted against NO density.

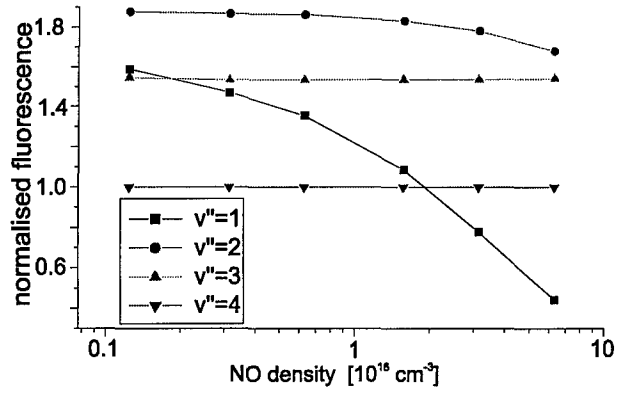

Fig.16 Normalised fluorescence versus NO density showing reabsorption effects for lower v''.

One sees here that while the strong reabsorption for emission to v" = 1, even at low densities, makes fluorescence measurements to this level unsuitable for TLT, fluorescence to levels v" = 3 and 4 is unaffected. In fact, for the estimated HEG NO densities lying in the range 1 - 8 x 10^{15} cm^{-3} (Fig. 7), and for the given HEG test section geometry, reabsorption of fluorescence to the levels v" = 2, 3 or 4 is at most 1%. To be sure of minimising these effects, only v" = 3 and 4 fluorescence is used in all further TLT work.

5.4 Linear fluorescence

Fig. 17 shows reference cell corrected fluorescence signals in the test cell (setup as in Fig. 10) at three temperatures as a function of NO pressure for transitions 1. (open symbols) and 2. (closed symbols), as defined in chapter 5.1. Symbols: circles and diamonds refer to measurement of fluorescence transitions $D^2\Sigma^+(v' = 0) \rightarrow X^2\Pi(v" = 3,4)$ and $A^2\Sigma^+(v' = 0) \rightarrow X^2\Pi(v" = 3,4)$. Even though there is a linear relationship between fluorescence intensity and NO density in the range relevant for the HEG free stream (0.1 - 0.8 x 10^{16} cm^{-3}), one can see that this relationship is not held at higher densities. Here quenching and, especially at high laser power densities, ASE (see chapter 2.3) play a role.

The lesson here for HEG free stream TLT work is that low laser power densities should be used, even at the trade-off of spatial resolution (no laser

sheets). This will be further exemplified in chapter 5.6.

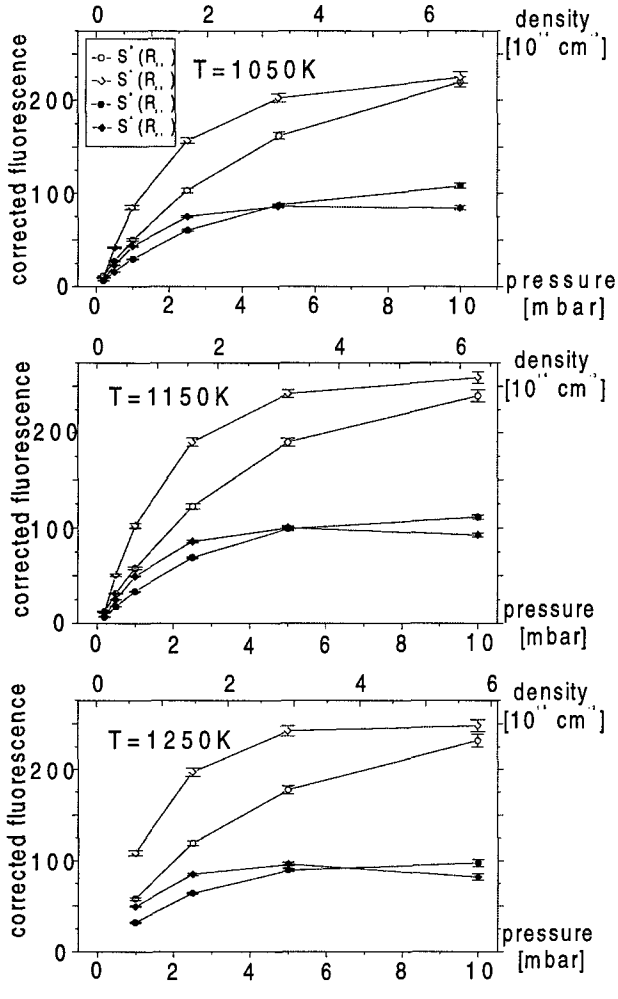

Fig. 17 Corrected fluorescence signals versus NO pressure for three temperatures (Ref. 5).

5.5 Quantum yields

Quantum yield was defined in chapter 2.3 as $q_F = \frac{A_{21}}{A_{21} + Q_{21}}$. Fig. 18 shows a calculation of q_F as a function of NO density for three temperatures for the states $D^2\Sigma^+$ (v' = 0) and $A^2\Sigma^+$ (v' = 0). Literature values (see Ref. 1) for quenching cross sections $\sigma(A) = 44$ Å^2 and $\sigma(D) = 83$ Å^2 were used. This shows that $q_F[\varepsilon(0,v'')] \geq 0.95$ for all temperatures for HEG free stream NO concentrations.

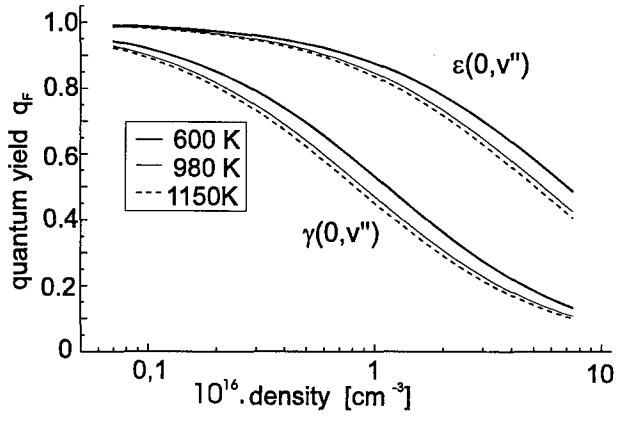

Fig.18 Calculated quantum yields for NO D and A states versus NO density at three temperatures (Ref. 5).

Even if $q_F << 1$, a glance at the derivation of the equations for TLT in chapter 2.4 had assumed that $q_{F,1} = q_{F,2}$, so that the actual values of q_F didn't matter, as long as they were the same for both states |1> and |2>. This is an important requisite for use of TLT as used here. Unfortunately very little is known about quantum level dependence on quenching of these NO excited states, so that tests had to be carried out to determine $\sigma(A)$ and $\sigma(D)$, using our familiar transitions 1 and 2.

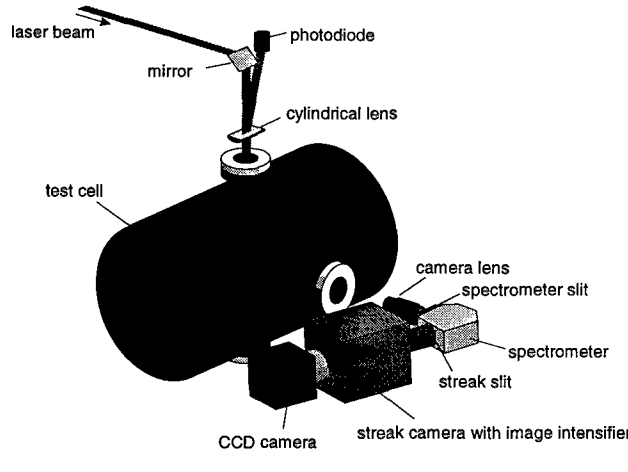

Fig.19 Apparatus to measure NO fluorescence lifetimes and quenching using a streak camera.

To do this, the experimental setup, shown in Fig. 19, coupled the test cell with a detection system consisting of a UV lens, a spectrometer and a fast streak camera capable of time resolved

fluorescence measurements with nanosecond resolution (Ref. 4). With this setup time resolved fluorescence measurements of NO at two temperatures (1157 and 1277 K) and various gas pressures (100 Pa- 20 kPa) for mixtures of NO and N_2 between 1 and 100% were carried out. Typical results are shown in Fig. 20.

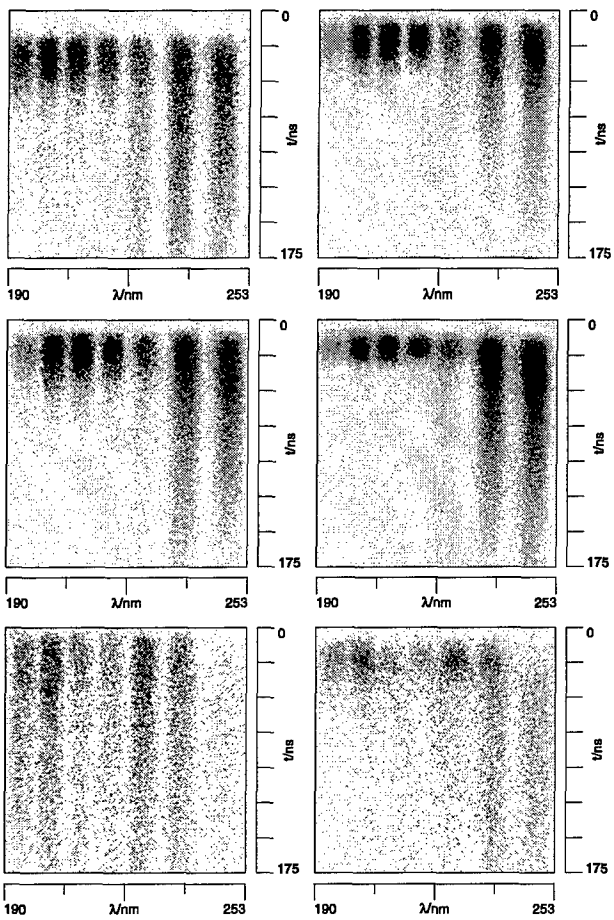

Fig.20 NO quenching seen in different time resolved fluorescence measurements (see text).

Here the horizontal axes represent wavelength from 190 - 250 nm, the vertical axes time from 0 to 175 ns. *Upper traces*: transition 1, 1227 K, NO 200 Pa (left), NO 1 kPa (right). *Middle traces*: transition 2, 1157 K, NO 500 Pa (left), NO 500 Pa + N_2 19.5 kPa (right). *Lower traces (for comparison)*: transition (3,0) R11 (43.5), 1157 K, NO 500 Pa (left), NO 500 Pa + N_2 19.5 kPa (right). Functions of the form $f_{theor}(t) = I_0 e^{-t/\tau_{nat}} + B$ (I_0 is the original fluorescence signal intensity at t = 0, τ_{nat} the natural fluorescence lifetime and B the background signal) were fitted to the experimental plots in Fig. 20 at late times to avoid having to carry out complex deconvolutions with the laser pulse form ($\tau_{1/e}^{laser} \cong$ 17 ns). Fluorescence lifetimes τ are then plotted logarithmically versus NO pressure (mbar) (Stern-Volmer plots), from which the natural upper state lifetimes τ_{nat} and quenching cross sections σ_X (X = NO, N_2) can be determined (see Ref. 4). A typical Stern-Volmer plot for measurement of fluorescence $A^2\Sigma^+(v' = 0) \rightarrow X^2\Pi(v'' = 1,2)$ after excitation using transition 1 at temperature 1157 K and with pure NO is shown in Fig. 21. The following table shows the results for τ_{nat}, σ_{NO} and σ_{N2} for the $D^2\Sigma^+$ (v' = 0) state for the two rotational levels J = 27.5 and 17.5, obtained from an analysis of a multitude of Stern-Volmer plots as in Fig. 21.

	ε(0,1) R_{22}(27.5)		**ε(0,1) R_{21}(17.5)**	
	1157 K	*1277 K*	*1157 K*	*1277 K*
τ_{nat} **(ns)**	16.5	17.5	20.7	18.8
σ_{NO} **(Å^2)**	46	64	75	62
σ_{N2} **(Å^2)**	42	42	30	50

One sees that σ_{NO} and σ_{N2} are different for the two rotational levels! Having obtained these experimental values, and using calculated values of NO and N_2 concentrations in the HEG free stream, one can now finally assess the inaccuracy introduced by the assumption $q_{F,1} = q_{F,2}$ made in chapter 2.4. The quench rate of NO by species i is given by $Q_{21}^i = \sum_i N_i \sigma_i v_i$, where N_i = concentration of species i, σ_i = quenching cross section and v_i = average velocity of species i ($v_i = \sqrt{8kT/\pi\mu_{NO-i}}$, k = Boltzmann's constant, T = temperature, μ_{NO-i} = reduced mass of collision pair NO and species i). Using measured values of σ_{NO} and σ_{N2} to determine Q_{21} and therefrom q_F, then ratios of $q_{F,1}/q_{F,2}$ can be determined for the HEG run conditions. These are summarised in the following table:

HEG condition		**I**	**II**	**III**	**IV**
$q_{F,1}/q_{F,2}$	500 K	1.05	1.08	1.05	1.09
	1157 K	1.08	1.12	1.08	1.12
	1277 K	1.08	1.13	1.09	1.13

It can be seen here that the assumption that $q_{F,1} = q_{F,2}$ would lead to errors in forming fluorescence ratios of about 5 - 13%; in the best case, one can ignore this effect and accept the larger error, in the worst a correction for $q_{F,1}/q_{F,2}$ would need to be made.

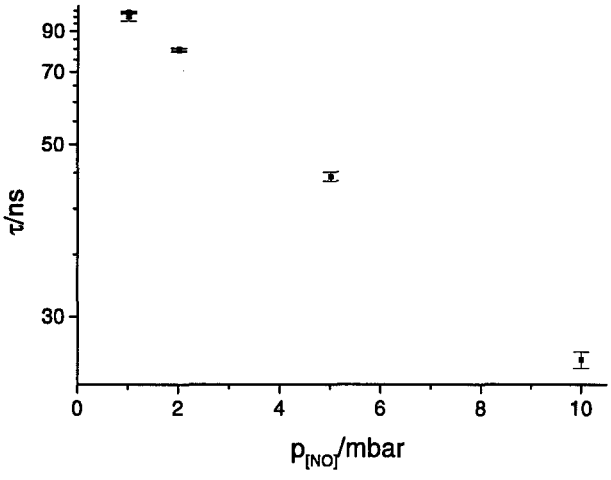

Fig.21 Stern-Volmer plot for NO A → X fluorescence at 1157 K.

5.6 Laser beam transmission

Absorption of the laser beam on its path to the test volume not only falsifies results, but, if severe enough, can reduce fluorescence signals to below detectable levels. Laser beam transmission measurements for transitions 1 and 2 in the test cell with NO densities below 1 x 10^{16} cm^{-3} and at the highest temperature (1150 K) showed that there is a negligible effect. This is mainly due to the use of NO transitions arising from high vibrational (v" = 1) and rotational (J" = 17.5, 27.5) levels, which, even at 1150 K, are thermally not strongly populated (see chapter 2.2). This is one advantage of using ε-band rather than γ-band excitation of NO - the latter originates from the v" = 0 level, where considerable laser beam absorption occurs.

There is another source of laser beam extinction which causes problems - scattering by particulate matter in the flow. This is a typical problem with high enthalpy facilities and was referred to before (chapter 4) as producing the strong emission behind shocks. Its effect is the same as that due to absorption - less of the laser beam reaches the test volume. This is illustrated most graphically in Fig. 22, where percent transmission for the two transitions 1 (open circles) and 2 (filled circles) are plotted for eight shots in sequence of performance in HEG at low (~40 MPa) and high (~100 MPa) pressure conditions. (The high pressure conditions are identified in the figure with Roman numerals II and IV.)

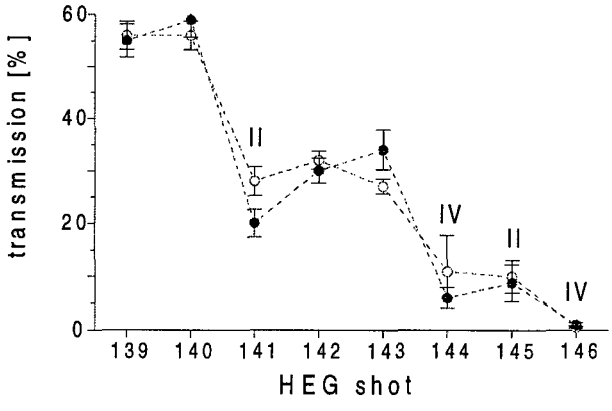

Fig.22 A sequence of HEG shots showing reducing transmission due to flow contamination.

At the first shot (#139) transmission was only about 55%, and by the last shot (#146) it was almost down to 0%. The drastic effect of high pressure shots can also be seen; the transmission drops rapidly. This correlates with the findings that ablation of materials in the tunnel is much greater with high pressure shots. LIF measurements at these high pressures are most difficult, either one needs to measure transmission *in situ*, or choose test times very early in the flow before the contamination arrives.

5.7 Saturation of fluorescence

If one pumps an NO transition too hard (laser power density is too high and/or quantum level population is very low and/or transition moments (Einstein coefficients) are very large), it is possible to empty the level during the time of the laser pulse, so that further incoming photons don't lead to a further excitation of NO. The linear dependence between fluorescence signal and laser power no longer holds, and, in the worst case, further increases in laser power lead to no further fluorescence signal increase - complete saturation has occurred. Our transitions 1 and 2 have Einstein

B coefficients of 999 and 406 cm J^{-1}, respectively, and both rotational levels J" = 17.5 and 27.5 are quite high and therefore not highly populated (see Fig. 4). Therefore, at higher laser power densities, one may expect saturation effects to occur, more so for the transition 1 than 2. This is indeed the case, as is shown in Fig. 23 (from Ref. 5), where fluorescence signal measured in the test cell (1100 K with 500 Pa NO) is plotted against laser energy density for both transitions 1 and 2 (for comparison, the dashed line shows the expected behaviour for linear LIF).

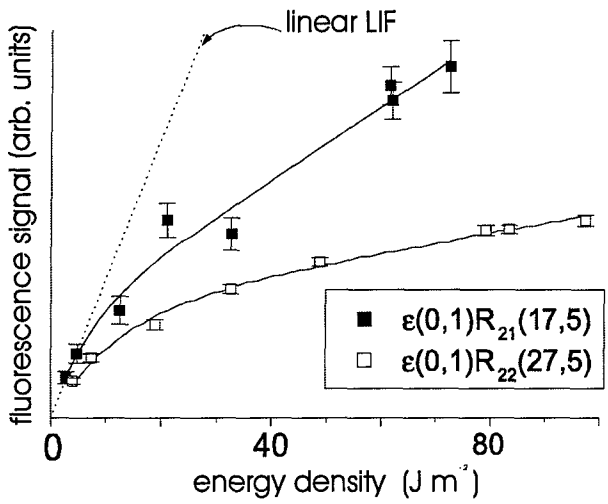

Fig.23 Fluorescence signal vs. laser energy density for NO at 1100 K and 500 Pa (Ref. 1).

Deviation from linear LIF starts to become severe at energy densities above about 10 J m^{-2} (which corresponds to a laser power density of ~700 MW m^{-2}). To avoid saturation effects, energy densities below this value should be used. The trade-off for linear LIF, especially for transition 2, is the reduced fluorescence signal intensity, which may be critical with single shot TLT in environments such as HEG where signals are quite weak anyway.

5.8 Fluorescence signal Boltzmann plots

Armed with what has been learnt so far, the best proof of TLT in the test cell is to plot fluorescence signal ratios for transitions 1 and 2 logarithmically against inverse temperature (Boltzmann plot) - the slope should be equal to ΔE/k, where ΔE is the energy separation of the two energy levels from which excitation occurred. For our transitions 1 and 2, ΔE/k = 1310 K. Fluorescence measurements were carried out (Ref. 5) at four different NO concentrations n_{NO} (1, 3, 5 and 8 x 10^{15} cm^{-3}) and with 5, 10 and 100% NO/N_2 mixtures. Boltzmann plots are shown in Fig. 24 for only two n_{NO} (upper plot - n_{NO} = 3 x 10^{15} cm^{-3}; lower plot - n_{NO} = 8 x 10^{15} cm^{-3}). Lines of best fit for each mixture are

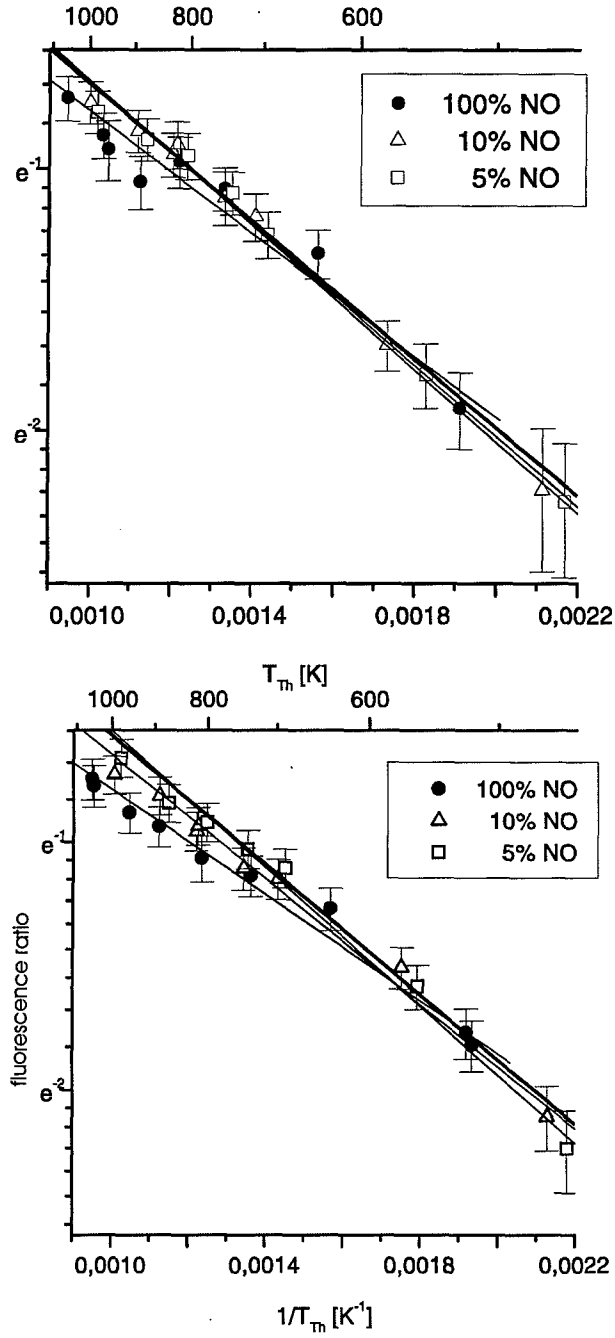

Fig.24 Boltzmann plots for two NO densities (upper - 3 x 10^{15} cm^{-3}; lower - 8 x 10^{15} cm^{-3}) and different NO/N_2 percentages.

shown, as is the expected result with the slope 1310 K. Deviations can be seen to be larger for the higher n_{NO}.

If one now plots the slopes of the fitted lines in Fig. 24 for each mixture as slope (in K) versus NO density, one obtains the result in Fig. 25. This encouraging result shows that over the n_{NO} range 1 - 8 x 10^{15} cm^{-3} (HEG free stream), the deviation from 1310 K is quite small for 5 and 10% mixtures (which also corresponds to the HEG case). The 100% mixture result lies furthest from the expected line; the reasons are not clear, but may be due to experimental difficulties in dealing with low gas pressures in the test cell and concommitant uncertainties in the temperature.

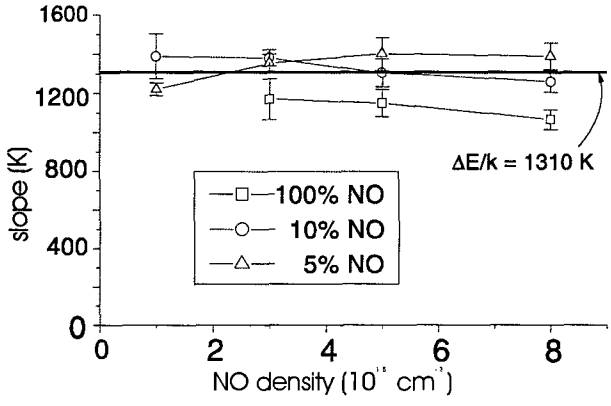

Fig.25 Measured Boltzmann plot slopes from Fig. 24 versus NO density at different NO/N_2 percentages.

6. LIF RESULTS IN HEG - FREE STREAM FLOW

LIF measurements were carried out in the HEG free stream flow with various run conditions to determine rotational and vibrational temperatures using TLT. T_{rot} is of interest since it represents the "inner" temperature most likely to mirror the gas translational temperature T_{trans}, which is difficult to measure with any accuracy by other means (although line-of-sight absorption techniques using laser diode absorption of NO and of a seed species rubidium have delivered translational temperatures, albeit only to an accuracy of ±20% - see Ref. 6). For T_{vib}, based on nozzle flow calculations using a simple Landau-Teller approach for vibrational relaxation of NO, T_{vib} is believed to lie above T_{trans}; vibrational relaxation freezes early in the nozzle flow.

6.1 Rotational temperature T_{rot}

Using the experimental setup shown in Fig. 9, and with the two detection systems (one for each laser) configured as OMA's, spectrally resolved fluorescence spectra were obtained in the HEG free stream at various run conditions after laser excitation of NO using transitions 1 and 2. Measured fluorescence spectra are shown as fluorescence intensity in counts against wavelength for transition 1 (left hand side) and 2 (right hand side) in Fig. 26. Also indicated are shot conditions (I - IV - see Fig. 7) and shot numbers 139 - 146.

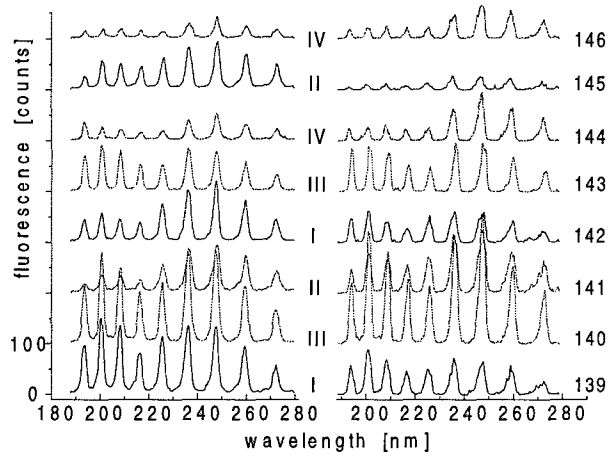

Fig. 26 Measured NO fluorescence spectra in HEG for eight shots at four conditions.

These results were analysed using the method outlined in chapter 2.4 for TLT to yield T_{rot} in the HEG free stream, as shown in the following table:

shot	cond	p_0 (MPa)	h_0 (MJ kg^{-1})	N_{NO} (10^{15} cm^{-3})	T_{theor} (K)	T_{rot} (K)
139	I	38.8	21.8	0.96	763	710
140	III	44.7	13.2	3.85	552	620
141	II	84.9	22.7	2.61	1026	*
142	I	38.8	21.0	1.10	791	980
143	III	40.0	12.0	3.86	475	630
144	IV	105	11.6	1.04	559	*
145	II	68.3	21.0	2.48	903	*
146	IV	97.3	14.4	7.63	703	480

(* temperature evaluation not possible.)

Reservoir pressure p_0 and T_{rot} were measured, specific enthalpy h_0, NO concentration N_{NO} and temperature T_{theor} were calculated using a chemical non-equilibrium computer code for nozzle flows (see Ref. 1). The agreement between T_{rot} and T_{theor} is not good, there being scatter in both directions. The main reason for this is that these measurements were performed before the substantial tests on TLT in the test cell (chapter 5) had been carried; these latter tests were indeed triggered by the poor agreement between measured and theoretical temperature results.

6.2 Vibrational temperature T_{vib}

As mentioned in chapter 5.1, there is a chance overlap of two NO transitions, one originating in the v" = 0, the other in the v" = 1 vibrational states:

3. $\gamma(3,0)\ R_{11} + Q_{21}$ (45.5) 51746.7 cm^{-1}
4. $\gamma(4,1)\ R_{11} + Q_{21}$ (27.5) 51746.7 cm^{-1}

Both transitions 3 and 4 are excited by tuning the laser to 51746.7 cm^{-1}. This is shown pictorially in Fig. 27 in an energy level diagram which includes the rotational manifolds.

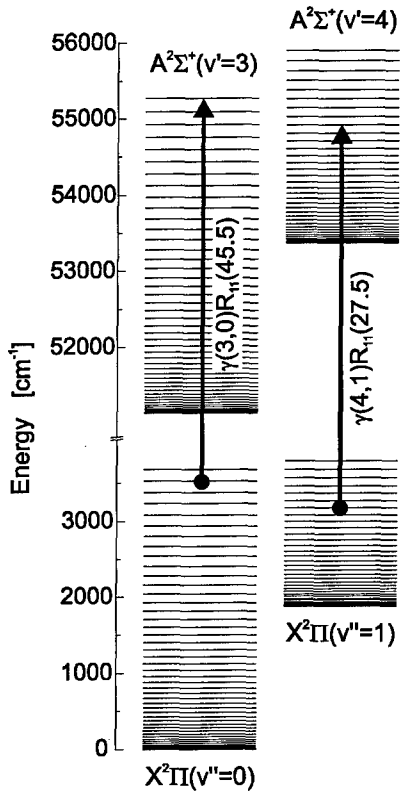

Fig. 27 Chance overlap of two NO transitions used for vibrational temperature determination (Ref. 1).

The measured fluorescence spectrum $F_\gamma(\lambda)$ is made up of the sum of components from the $A^2\Sigma^+$ (v' = 4) and $A^2\Sigma^+$ (v' = 3) upper states, $F^{27.5}_{\gamma(4,v")}(\lambda)$ and $F^{45.5}_{\gamma(3,v")}(\lambda)$, respectively, weighted with linear, temperature-dependent factors $\beta'(T)$ and $\alpha'(T)$:

$$F_\gamma(\lambda) = \alpha'(T)\, F^{45.5}_{\gamma(3,v")} + \beta'(T)\, F^{27.5}_{\gamma(4,v")}.$$

Since the two transitions 3 and 4 are coincident, it is not possible to measure them separately. However, neighbouring transitions from the same band can be used to measure similar single line spectra at various temperatures in the test cell, from which the factors $\alpha'(T)$ and $\beta'(T)$ can be determined. A further complication is the possible difference (thermal non-equilibrium) between T_{rot} and T_{vib} in HEG (in the test cell they are the same, of course). The relative population $\xi(T_{vib}, T_{rot})$ of the two lower (v",J") states, $X^2\Pi$(v" = 1, J" = 27.5, F_1 and $X^2\Pi$(v" = 0, J" = 45.5, F_1 is related to T_{vib} and T_{rot} by the following equation (where the constant is to be determined from the test cell calibration measurements at different temperatures):

$$\xi(T_{vib}, T_{rot}) = \frac{f(v=1, J=27.5, F_1)}{f(v=0, J=45.5, F_1)} = const. \frac{\beta(T)}{\alpha(T)} = 0.61 \cdot e^{\left[\frac{\Delta E_{vib}}{kT_{vib}} + \frac{\Delta E_{rot}}{kT_{rot}}\right]}$$

Fig. 28 shows a calculation for T_{rot} = 800 K and various T_{vib} between 800 and 2500 K, where one can see how the fluorescence spectra change. Also indicated in the figure with two arrows (↓) are two fluorescence lines, one being sensitive, the other insensitive to temperature variation.

A comparison between a measured fluorescence spectrum in the HEG free stream and one calculated using the above-described method is shown in Fig. 29. The arrow (↓) shows the excitation wavelength.

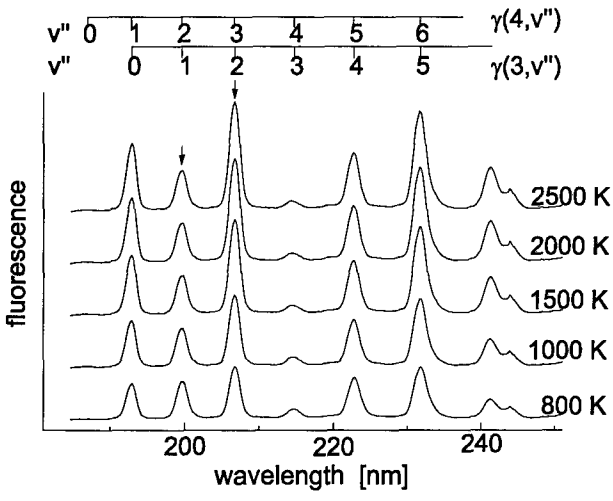

Fig.28 Calculated NO fluorescence spectra at T_{rot} = 800 K at various vibrational temperatures.

The agreement between measured and calculated spectra is quite good. From this fit a value for the relative populations of both levels could be determined:

$\xi(T_{vib}, T_{rot}) = 0.7 \pm 0.2.$

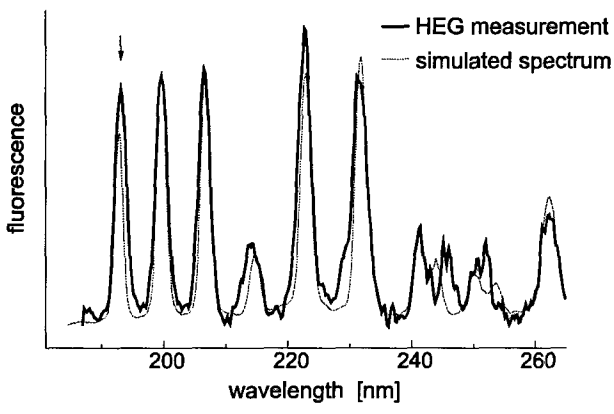

Fig.29 Comparison between measured (in HEG) and calculated NO fluorescence spectra obtained from simultaneous excitation by one laser.

If T_{rot} were known in HEG, then T_{vib} could be determined. Since both for the present must be treated as unknowns, one can represent this result pictorially as a contour plot of $\xi(T_{vib}, T_{rot})$ as a function of T_{vib} and T_{rot}. This is done in Fig. 30.

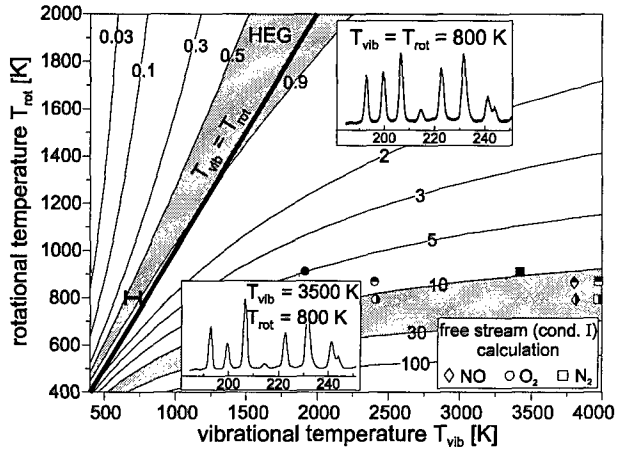

Fig.30 Contours of relative populations $\xi(T_{vib}, T_{rot})$ as a function of T_{vib} and T_{rot}.

In this figure a family of contours for values of $\xi(T_{vib}, T_{rot})$ lying between 0.03 ($T_{rot} >> T_{vib}$) and 100 ($T_{rot} << T_{vib}$) has been plotted. The thermal equilibrium case, $T_{vib} = T_{rot}$, is plotted as a straight line, along with an inserted spectrum for the case $T_{rot} = T_{vib}$ = 800 K. The grey region labelled HEG represents the result as measured (0.7 ± 0.2) with no assumption regarding the value of T_{rot}. If one assumes T_{rot} = 800 K, the error bar (|—|) represents the range of measured and predicted values of T_{vib}. The symbols in the figure for (T_{vib},T_{rot}) represent values calculated by various workers (see Ref. 1) for NO, O_2 and N_2 vibrational non-equilibrium - all predict $T_{vib} >> T_{rot}$. For comparison, the calculated fluorescence spectrum for the case where T_{vib} = 3500 K and T_{rot} = 800 K is inserted in the figure. Here values for $\xi(T_{vib}, T_{rot})$ would lie between 5 and 100 (!), which is well above the measured value of 0.7 ± 0.2. Although the results would seem to indicate thermal equilibrium, there are some reservations: above all, only two levels with two low v" (with small Δv") and two high J" (with large ΔJ") could be interrogated. Whether these are representative of the distribution over all levels is not known. Furthermore it is known that non-equilibrium distributions amongst vibrational and rotational levels exist in rapidly expanding gas flows (see Ref. 1).

7. LIF RESULTS IN HEG - MODEL FLOWS

Many LIF measurements have been carried out in HEG, leading either to spectrally-resolved fluorescence spectra or 2D field measurements of fluorescence. The former have been used to study the free stream and also to ascertain how to obtain sufficient fluorescence signals from behind strong shocks; the latter have yielded information on flow visualisation (shock positions) and 2D resolved temperature field measurements around models in the HEG test flow. The results of tests with these models - HERMES space glider, cylinder, sphere, blunted cone (planetary probe) and the Japanese space glider HOPE (HII orbital plane) - are presented here.

7.1 HERMES - European space glider

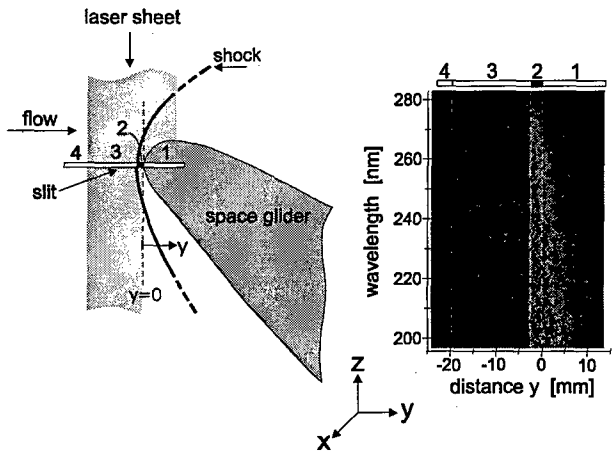

Fig.31 LIF measurements on HERMES in HEG (condition II).

In the late 1980's and early 1990's HERMES was a joint European development for a space transporter. Tests with models were carried out in HEG at conditions I and II. One laser, formed to a sheet, was made to pass in front of the model, tuned to a strong NO absorption line. The fluorescence emission was captured with a UV lens and focussed onto the OMA entrance slit (as in Fig. 9), which was placed transverse to the sheet. Fig. 31 (left hand side) shows the experimental setup.

This configuration affords a 1D spatial resolution along the slit. In the results of these measurements for an HEG shot at condition II, four regions can be identified, as shown in Fig. 31 in the experimental setup and in the experimental results (right hand side): 1. Region of shock heated gases where laser is blocked by model; 2. Behind the shock with laser excitation of NO; 3, In the free stream, with laser beam; 4. In the free stream, no laser beam. (The experimental result is an image, as recorded on the ICCD camera, with spectrometer dispersion (i.e. wavelength) in the vertical direction and spatial resolution (along the slit) in the horizontal.) The expected NO fluorescence spectrum can clearly be seen in region 3, whereas region 2 is harder to resolve.

By laying vertical profiles through the regions 1, 2 and 3 for the result shown in Fig. 31 and for two other HEG shots, the spectra shown in Fig. 32 were obtained.

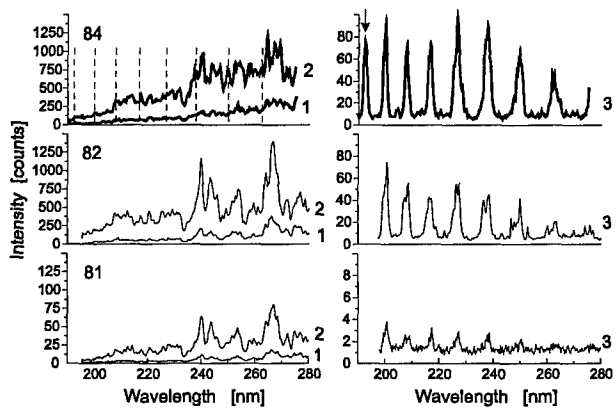

Fig.32 Spectra from HERMES for regions 1, 2 and 3 (see Fig. 31) for three HEG shots.

Shots 81, 82 and 84 were at conditions I, I and II, respectively. Camera gates were between 30 and 50 ns. Laser excitation occurred at the line wavelength shown in the top right hand spectrum by a vertical arrow (↓). In shots 82 and 84 (and less so in 81) one can clearly see the NO fluorescence spectrum after exciting transition 1 in region 3. For all three shots there is no indication of a fluorescence signal in region 2 at those wavelength positions (indicated by dashed lines) where it should occur. There are a few possible reasons for this: first, the very limited resolution afforded by the OMA setup (slit width was 280

μm) coupled with the very small shock stand-off distance (<3 mm) in the stagnation region in front of HERMES may prevent the weak fluorescence lines from being seen. Secondly, at the higher densities behind the shock, fluorescence quenching would also play a more major role. Finally, the strong emission behind shocks (see chapter 4) may mask any weak NO fluorescence signals. To overcome the spatial resolution problem, tests with a cylinder having a larger shock stand-off distance were carried out.

7.2 Circular cylinder

A cylinder with diameter 90 mm and length 500 mm was placed in the flow with its axis perpendicular to the flow direction. The optical set-up was identical to that shown for HERMES (chapter 7.1). Laser excitation occurred either via transition 1 or 2, or via a strong group of mixed lines ($\varepsilon(0,1)$ $Q_{11}(32.5)$ + $P_{21}(32.5)$ + $R_{21}(21.5)$ + $R_{11}(26.5)$ + $Q_{21}(26.5)$). Gates were either 50 or 300 ns. The experimental set-up and one of the recorded results (shot 236, group of lines, 150 mJ, 50 ns gate) are shown in Fig. 33.

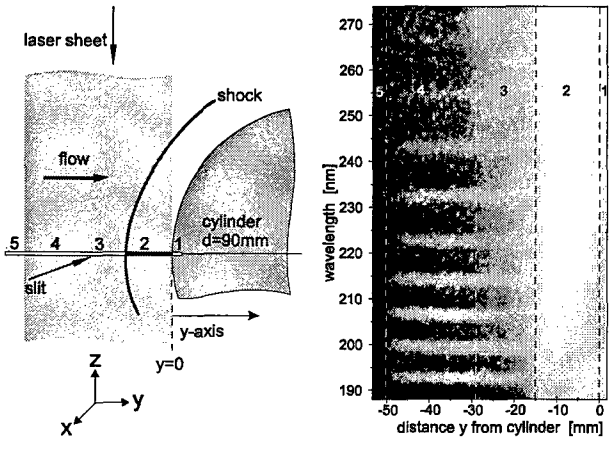

Fig.33 LIF measurements on a cylinder in HEG.

Here five regions are identified, the free stream flow region with laser beam (region 3. In Fig. 31) being further split into two regions. In region 3, even though one can see the NO fluorescence lines, they start to become overlapped with background emission at the higher wavelengths. For two shots 235 (transition 1, laser energy 50 mJ, 300 ns gate) and 236 (group of lines, 150 mJ, 50 ns), vertical spectral profiles for regions 2, 3 and 4 are shown in Fig. 34.

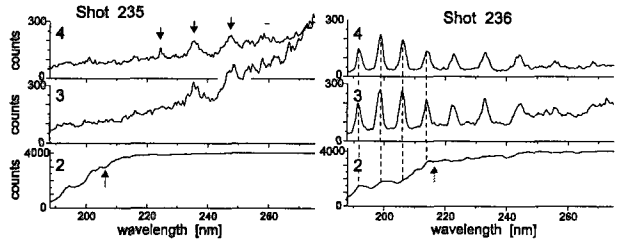

Fig.34 Spectra from the cylinder for regions 2., 3. And 4. (see Fig. 33) for two HEG shots.

Region 2 in both shots 235 and 236 is sooner or later saturated (commencing at position of vertical arrow ↑); even before saturation, no fluorescence lines are to be seen. One reason for this is the width of the laser sheet (0.5 mm) relative to the integrated length over which the background emission is seen (500 mm). Even the small camera gate of shot 236 was not sufficient to improve significantly the fluorescence-to-background emission ratio. Region 3 for shot 236 shows the free stream florescence lines, as in region 4, but overlapped especially at higher wavelengths with the background emission of region 2, even though one is in front of the shock! The region 2 emission is so overpowering and intense that it either scatters off matter in the free stream upstream of the shock, or by blooming or other optical effects extends into the upstream region. Due to its long integration length and the narrow laser sheet depth, the cylinder is not suited for LIF behind the shock.

7.3 Sphere

To reduce the long integration lengths of the cylinder (chapter 7.2) and increase the laser depth, sphere (radius 80 mm) tests with expanded laser beams were carried out. Three shots, all at condition I, all with one laser (90 mJ) fixed on the group of lines (see chapter 7.2) and with gates from 5 to 20 ns were carried out. In shot 259 the laser sheet was focussed to a sharp waist, in 260 and 261 the beam was expanded to a size of 50 x 21 mm^2, with the 50 mm being in the direction of integration with the cameras. This is shown in Fig. 35, side-on view top right, and front-on view

bottom left. Two OMA slit configurations were used, one transverse to the laser beam (as in Figs. 31 and 33), and one along the beam direction.

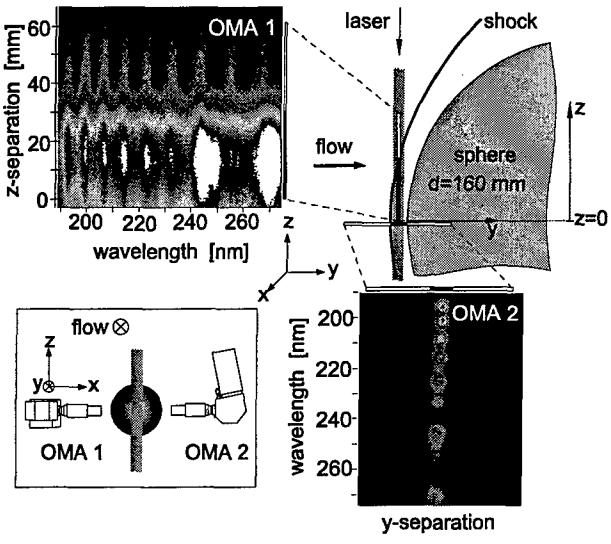

Fig.35 LIF measurements on a sphere in HEG using two different OMA slit alignments.

The results for shot 261 are also shown for both OMA configurations, where, in both cases, one can see NO fluorescence behind the shock. This is especially evident where the slit is in laser beam direction, where fluorescence from the free stream can also be clearly seen. This is the first recorded case of measured NO fluorescence behind a strong shock at high enthalpies.

Spectral profiles for the free stream (1), for the transition region between free stream and shock in the slit configuration along the beam (2), as in (2) but in the shock region, and with slit configuration transverse to the laser beam (4) are shown for shots 259 (thin line), 260 (medium line) and 261 (bold line) in Fig. 36. Downward arrows (↓) indicate onset of partial camera saturation. Asterisks (*) indicate spectral regions where the emission is largely due to the background emission.

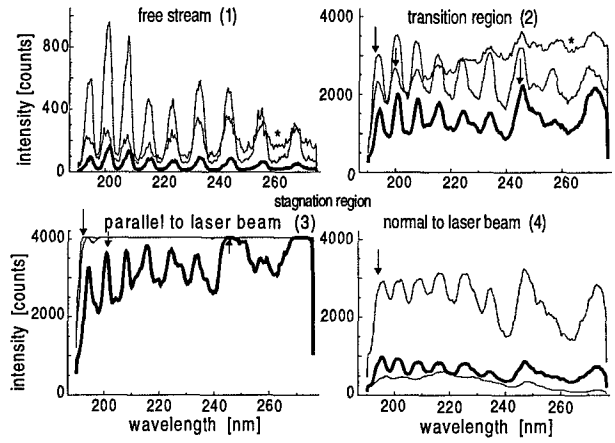

Fig.36 LIF spectral profiles for the four regions in three HEG shots.

These spectra show all too clearly the disadvantage of focussed (shot 259) compared with defocussed (shots 260 and 261) laser beams. An improvement in NO fluorescence/background emission intensity ratio by about a factor of 20 was chiefly due to: 1. Defocussing the laser beam; 2. Using a strong group of excitation lines; 3. Using very short camera gates; 4. Use of a sphere rather than a cylinder.

These tests were carried out with just one laser, so that an attempt at TLT could not be undertaken. Furthermore, to use TLT behind a shock with temperatures of over 6000 K, the presently available transitions 1 and 2 with their small $\Delta E/k$ value of only 1310 K are not suitable, Other transitions are needed, and since these are not accessible to the tunable ArF excimer lasers, other lasers will need to be used.

7.4 Blunted cone (planetary probe)

The blunted cone represents the forebody shape of a planetary probe. LIF was used (Ref. 7) to examine the flow wakes behind the cone; these are regions of interest since it is here that sensitive and delicate instrumentation is placed. There is also some concern regarding the influence of the model holder (sting) on the wake flow. The set-up for TLT measurements behind the cone is shown in Fig. 37. A shear layer separates the strong expansion at the edge of the cone from a re-circulation region in the corner formed by cone

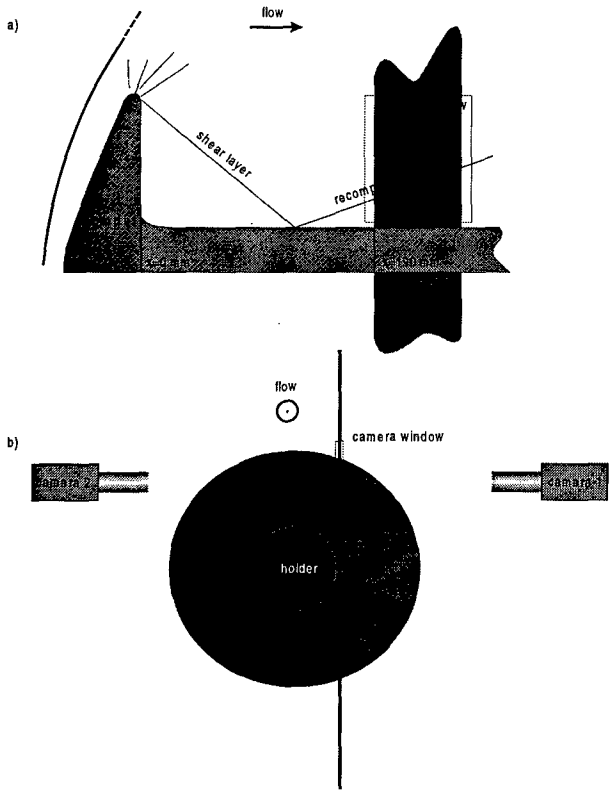

Fig.37 Experimental setup for LIF measurements in the wake of a blunted cone in HEG.

rear surface and sting. This shear layer impinges on the sting, where, to turn the flow, a weak re-compression shock is formed. PLIF measurements were performed in this region of the re-compression shock, with the configuration as shown. (Early tests in the region immediately behind the cone were not successful, even with the use of filters, due to the very strong background emission from behind the bow shock - at that stage, the methods leading to the successful results behind the sphere shock were not yet known.)

A 2D temperature plot and profile for the region shown in Fig. 37 is shown for shot 220 (condition III, test gas 30% N_2 + 70% CO_2) in Fig. 38.

One can faintly see the shock position in the inset 2D image (the shock is weak, the gas is quite "cold" and NO concentrations are quite low, so that fluorescence signals are very weak, leading to low S/N ratios are therefore poor signal quality). For the temperature determination a value of 1000 K has been assumed for the region upstream of the shock - this value has been obtained from calculations. Given this assumption, the LIF

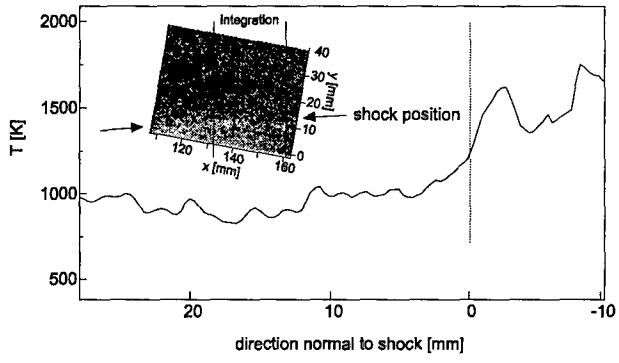

Fig.38 Visualisation of the compression shock in the wake of the blunted cone and evaluation of a temperature.

measurement shows that there is about a 1.6 temperature jump across the shock.

7.5 Japanese HII Orbital Plane (HOPE)

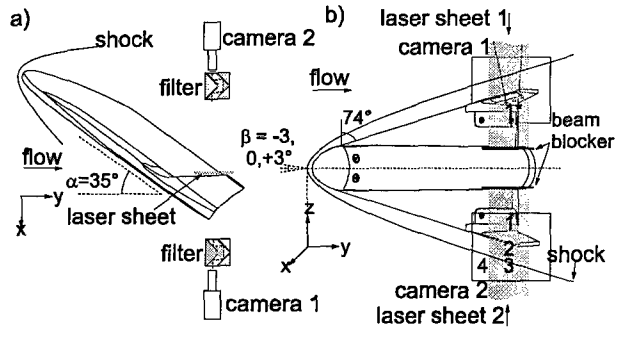

Fig.39 Experimental setup for LIF measurements on the HOPE power delta model.

PLIF measurements were carried out (Ref. 1, 4, 7, 8) on power delta and double delta shaped models as candidate shapes for the Japanese space glider HOPE. (This work was performed under contract to Kawasaki Heavy Industries.) Model angle of attack was 35°, three yaw angles of +3°, 0° and -3° were used, run conditions were I, II and IV, and laser transitions 1 and 2 were used in a two-laser set-up (Fig. 9) to record 2D NO fluorescence images. The experimental set-up for LIF for the power delta model, showing the configuration of the two laser sheets and the two ICCD's, is given in Fig. 39.

Here the laser sheets are brought in parallel to the flow direction just above the wing tip fins. Typical flow visualisation LIF images from both cameras (transitions 1 and 2) at yaw angles β of -3° (shot 198, condition IV) and +3° (shot 200, condition II) are shown in Fig. 40. The relative placement of the shock to the wing tip fin as β is changed can readily be seen.

The experimental set-up here doesn't allow both laser beams to probe the same region of the flow (see Fig. 39). Hence, to do TLT, one must either do repeat shots and hope for shot reproducibility, or use two symmetrical (β = 0°) regions in the one shot, and hope for flow homogeneity. Here the latter was chosen. A 2D result for shot 195 (condition I) for T_{rot} in the vicinity of the power delta wing tip fin is shown in Fig.41a and a plot of temperature as a function of distance from the shock front is shown in Fig. 41b.

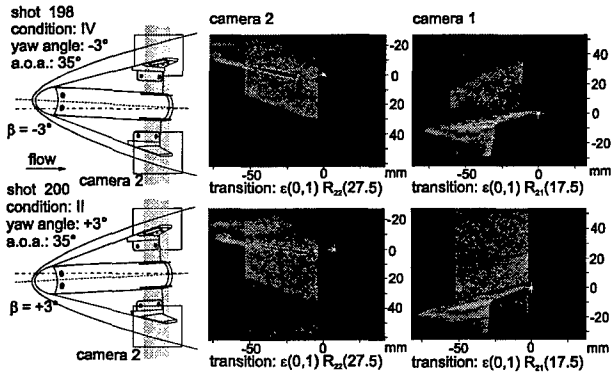

Fig.40 LIF flow visualisation for yaw angles +3 and -3° for the power delta model.

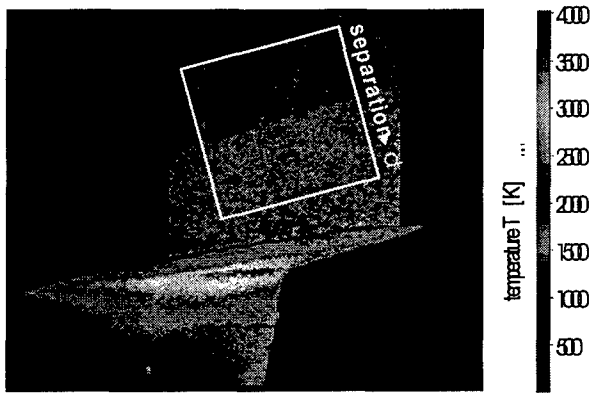

Fig.41a 2D temperature measurement using LIF in the vicinity of the HOPE power delta wing tip fin.

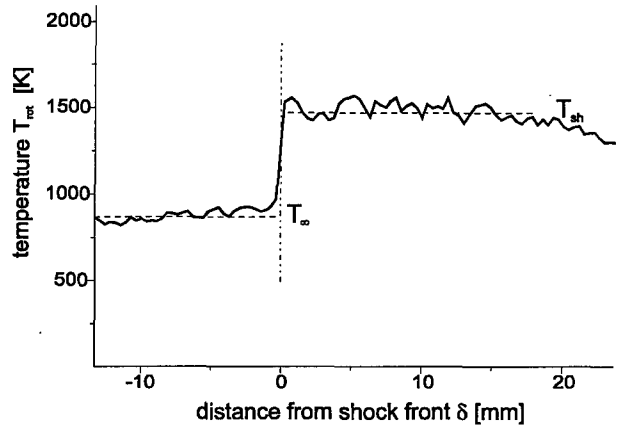

Fig.41b Temperature jump across the shock shown in Fig. 41a.

To obtain these temperature values, a free stream value of T_{rot} of 700 K (based on calculations for this condition) has been assumed.

A double delta model was also tested, but with a different laser beam configuration - here the laser beam was brought to pass just upstream of the wing leading edge, which meant that the laser beam and therefore the cameras had to be tilted. This is shown in Fig. 42.

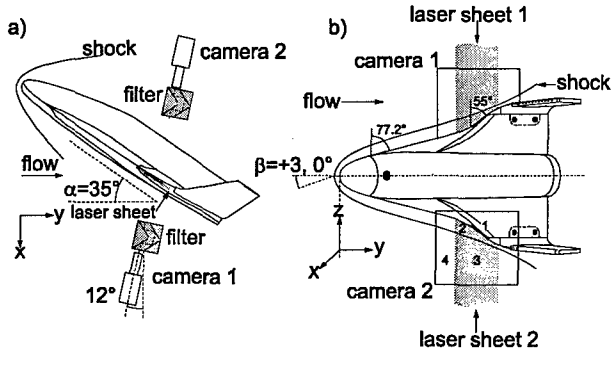

Fig. 42 Experimental setup for LIF measurements on the HOPE double delta model.

Typical results are shown in Fig. 43 for two shots at two different yaw angles: shot 204 (condition I, β = 0°) and 201 (condition I, β = +3°).

The shock stand-off distance from the wing leading edge as a function of β was measured over many HEG runs (shots 201 to 209) with different conditions. A summary of all double delta results is given in Fig. 44, where shock distances (in mm)

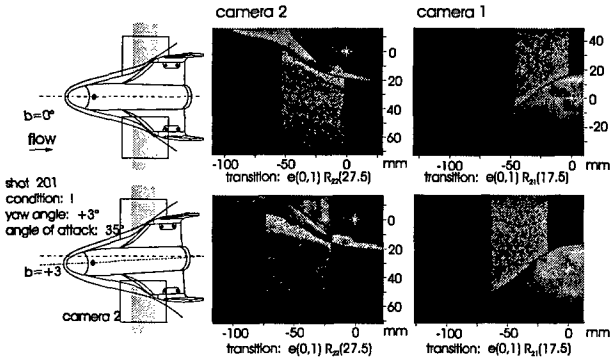

Fig.43 LIF flow visualisation for yaw angles 0 and 3° for the double delta model.

are plotted for the different HEG shots. (Yaw angles β = -3°, 0° and +3° are identified. Open symbols - condition I; half open symbols - condition II; filled symbols - condition IV. Squares - right wing camera 1; circles - left wing, camera 2. a, b -shock distance could not be determined.)

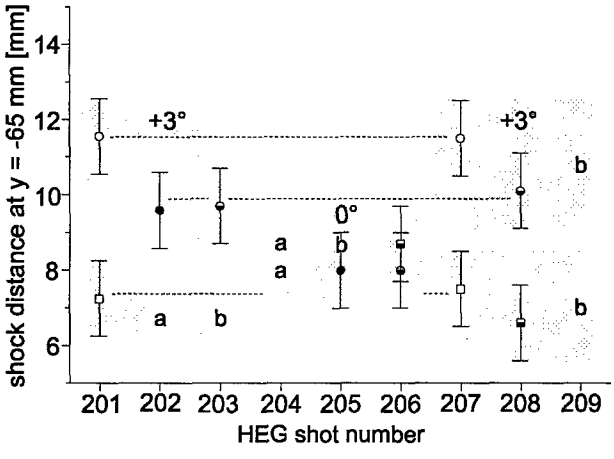

Fig.44 Distance from shock to wing leading edge for the double delta model for various HEG shots.

8. FLASH LAMP ABSORPTION IN HEG FREE STREAM FLOWS

The theoretical considerations in chapter 2 concerning the NO molecule, its spectroscopy, its level populations, considerations of thermal equilibrium, and TLT also apply here with this method. There are some major differences, however:- 1. It's an absorption technique, meaning line-of-sight integration along the direction of the flash lamp beam (LIF is spatially resolved); 2. Since the exciting source is broad-band, many NO absorption lines are probed, so that several level populations can be determined; 3. The flash lamp can operate at high repetition rates, so that time resolved spectra can be recorded during the flow.

Fig. 45 shows the University of Bielefeld experimental set-up for flash lamp absorption measurements of the HEG free stream flow. The flashlamp delivers a small (1 mm) 1 mJ pulse of short duration (100 ns) and at high repetition rates (100 kHz), with a sizeable proportion of its output in the UV. The beam is collimated, passed through the HEG test section normal to the flow axis and then focussed onto the entrance slit of an f9 spectrometer. This spectrometer contains an echelle grating as its dispersive element, which is used at very high order dispersion (>100), giving a very good wavelength resolution (0.0075 nm). Hence rotational lines can be resolved. The wavelength-dispersed spectrum from the lamp pulse is then recorded on an ICCD while a half frame transfer is occurring, thereby allowing a series of pulses to be recorded.

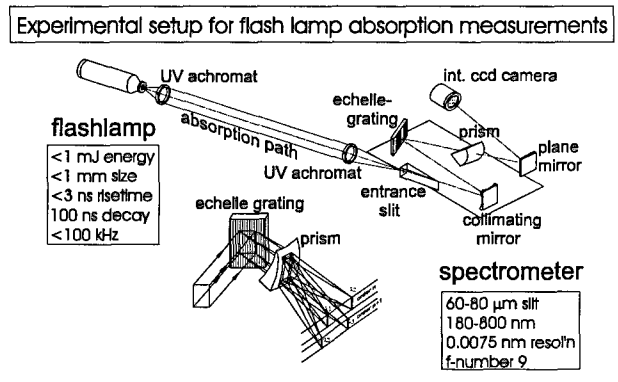

Fig. 45 Experimental setup for flash lamp absorption measurements in HEG.

Both low and high resolution spectra were recorded for two HEG shots, both at condition I. Fig. 46 shows a low resolution result for the wavelength range 210 - 240 nm.

At this resolution the rotational line structure cannot be resolved, but rather merges together to give the familiar vibrational band structure of NO. Three vibrational bands are seen in the measured spectrum (middle of figure), arising from γ(1,0),

γ(0,0) and γ(0,1) transitions. (This spectrum has been integrated over several flash lamp pulses to improve the S/N.) Inserted into the figure at lower

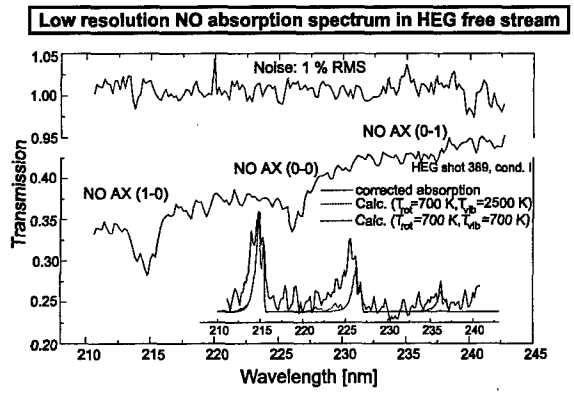

Fig.46 Low resolution flash lamp absorption measurement of NO in the HEG free stream.

right is the corrected measured absorption spectrum and two theoretical spectra for NO, one calculated for $T_{rot} = T_{vib} = 700$ K, and the other for $T_{rot} = 700$ K and $T_{vib} = 3500$ K. The major difference between the two calculated spectra is the appearance of the hot band at 236 nm when $T_{vib} = 3500$ K. (Hot bands arise from higher vibrational levels - here v" = 1 - which usually are only occupied when the gas is hot.) Even though the positions of the bands are predicted quite well, the agreement (goodness of fit) between experimental and calculated spectra is not very good - the top trace in Fig. 46 shows the residuals (least square differences) between calculated and experimental spectra. Furthermore, the hot band at 236 nm is not well enough resolved to be sure that T_{vib} is high.

A measured high resolution spectrum is shown in Fig. 47 (bold line plot). The wavenumber range as shown corresponds to a wavelength range of 227.0 - 225.5 nm.

Here the rotational structure of the γ(0,0) vibrational band is resolved. Also shown is a simulated spectrum for NO absorption calculated for $T_{rot} = 700$ K (grey line plot). The agreement is quite good, as shown in the χ^2 residuals plot in the lower right hand corner of Fig. 47; herefrom one would give a value for $T_{rot} = 650 \pm 50$ K. This can

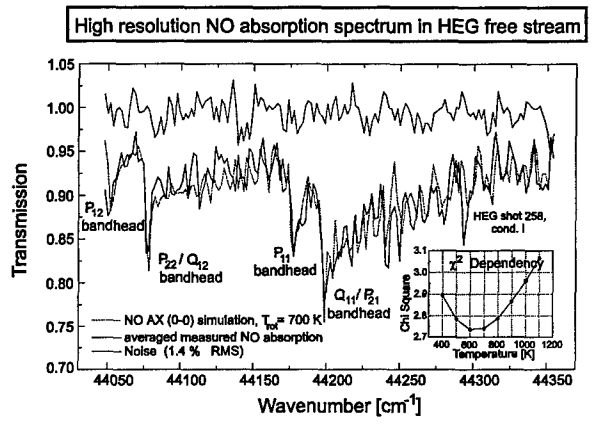

Fig.47 High resolution flash lamp absorption measurement of NO in the HEG free stream.

be compared with LIF values for T_{rot} of 710 K and 980 K (see chapter 6.1) and the theoretical value for T_∞ of 790 K (see Fig. 7).

ACKNOWLEDGEMENTS

The LIF work was carried out by a host of people working at the DLR: Dr. M. Wollenhaupt (who coordinated the LIF activities at HEG over several years and whose doctoral thesis forms the core part of this lecture), Dr. M. Scheer, M. Rosenhauer, T. Müller, J. Jourdan, J. Scholz and S. Hartung. The original laser apparatus for LIF was provided by LaVision 2D Meßtechnik GmbH (Göttingen, Germany). The flash lamp absorption technique, as used here, originates from the group of Prof. P. Andresen (University of Bielefeld) and was implemented in HEG by Dr. C. Niederbäumer (previously University of Bielefeld). Much of the funding for the LIF work, as well as for the LIF apparatus, was provided by the ESA through CNES.

REFERENCES

1. Wollenhaupt M. (1997) Einzelpuls Zwei-Linien-Thermometrie mit planarer laserinduzierter Fluoreszenz an NO-Molekülen in Hochenthalpieströmungen. *Dissertation, Faculty of Physics, University of Bielefeld.*

2. Eitelberg G. (1993) Calibration of the HEG and ist Use for Verification of Real Gas Effects in High Enthalpy Flows. *AIAA Paper 5170.*

3. Scheer M. (1994) Temperature and density measurements on hypersonic wind tunnels using laser induced fluorescence of NO, including a study of NO spectroscopy in the range 193 - 4 nm, using a novel heated cell. *Diplom thesis, Faculty of Physics, University of Göttingen. (DLR IB 223-96 A 32).*

4. Jourdan J. (1998) Zeitaufgelöste Messung der laserinduzierten Fluoreszenz von heißem NO zur Validierung der Zwei-Linien-Thermometrie für die Anwendung in Hochenthalpieströmungen. *Diplom thesis, Faculty of Physics, University of Göttingen. (DLR-IB 223 98 A 37.*

5. Hartung S. (1999) Laserinduzierte Fluoreszenz an heißem NO zur Anwendung der Zwei-Linien-Thermometrie an einer beheizbaren Zelle. *Diplom thesis, submitted to Faculty of Physics, University of Göttingen.*

6. Beck W.H. (1999) Spectroscopic Techniques for Measurement of Velocity and Temperature in the DLR High Enthalpy Shock Tunnel HEG. *Lecture in this RTO AVT/VKI Special Course on „"Measurements techniques for high enthalpy and plasma flows", 25. - 29. October, 1999.*

7. Rosenhauer M. (1996) Laserfluoreszenz Messungen an heißem NO im Göttinger Hochenthalpiekanal (HEG) und einer Kalibrierzelle. *Diplom thesis, Faculty of Physics, University of Göttingen.*

8. Müller T. (1996) Laserinduzierte Fluoreszenz von NO: Strömungsuntersuchung am Hochenthalpiekanal Göttingen (HEG) und Temperaturmessungen in einer heizbaren Kalibrierzelle. *Diplom thesis, Faculty of Physics, University of Göttingen.*